AD-A159 834 NONLINEAR MATERIALS FOR THE MILLIMETER SPECTRAL REGION 1/1
(U) HUGHES RESEARCH LABS MALIBU CA M KLEIN ET AL.
JUL 85 N00014-82-C-0226

UNCLASSIFIED F/G 20/3 NL

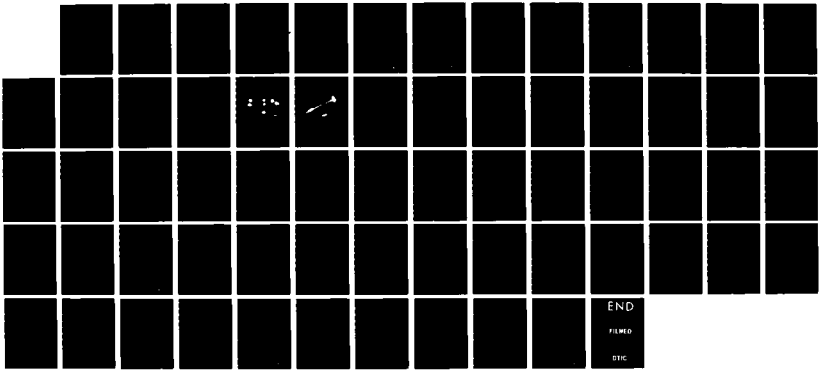

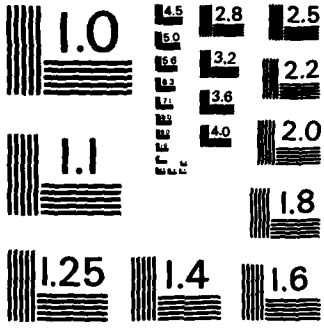

MICROCOPY RESOLUTION TEST CHART
NATIONAL BUREAU OF STANDARDS - 1963 - A

NONLINEAR MATERIALS FOR THE MILLIMETER SPECTRAL REGION

M.B. Klein, B.A. Wechsler, and D. Rytz

Hughes Research Laboratories
3011 Malibu Canyon Road
Malibu, CA 90265

July 1985

N00014-82-C-0226
Final Report
1 February 1982 through 28 February 1985

OFFICE OF NAVAL RESEARCH
800 North Quincy Street
Arlington, Virginia 22217

UNCLASSIFIED

SECURITY CLASSIFICATION OF THIS PAGE

AD-A159 834

REPORT DOCUMENTATION PAGE

1a. REPORT SECURITY CLASSIFICATION UNCLASSIFIED	1b. RESTRICTIVE MARKINGS
2a. SECURITY CLASSIFICATION AUTHORITY	3. DISTRIBUTION/AVAILABILITY OF REPORT
2b. DECLASSIFICATION/DOWNGRADING SCHEDULE	
4. PERFORMING ORGANIZATION REPORT NUMBER(S)	5. MONITORING ORGANIZATION REPORT NUMBER(S) Office of Naval Research
6a. NAME OF PERFORMING ORGANIZATION Hughes Research Laboratories 6b. OFFICE SYMBOL (If applicable)	7a. NAME OF MONITORING ORGANIZATION 800 N. Quincy St. Arlington, VA 22217
6c. ADDRESS (City, State and ZIP Code) 3011 Malibu Canyon Rd. Malibu, CA 90265	7b. ADDRESS (City, State and ZIP Code)
8a. NAME OF FUNDING/SPONSORING ORGANIZATION Office of Naval Research 8b. OFFICE SYMBOL (If applicable)	9. PROCUREMENT INSTRUMENT IDENTIFICATION NUMBER
8c. ADDRESS (City, State and ZIP Code) 800 N. Quincy St. Arlington, VA 22217	10. SOURCE OF FUNDING NOS. PROGRAM ELEMENT NO. / PROJECT NO. / TASK NO. / WORK UNIT NO.
11. TITLE (Include Security Classification) Nonlinear Materials for the Millimeter Spectral Region	
12. PERSONAL AUTHOR(S) M.B. Klein, B.A. Wechsler, and D. Rytz	
13a. TYPE OF REPORT Final 13b. TIME COVERED FROM Feb 82 TO Jun 85	14. DATE OF REPORT (Yr., Mo., Day) June 1985 15. PAGE COUNT 71
16. SUPPLEMENTARY NOTATION	
17. COSATI CODES FIELD / GROUP / SUB. GR.	18. SUBJECT TERMS (Continue on reverse if necessary and identify by block number)

19. ABSTRACT (Continue on reverse if necessary and identify by block number)

Nonlinear materials offer great promise for use in devices such as phase shifters, modulators, switches, and frequency multipliers at frequencies above 50 GHz. State-of-the-art phase shifters (using ferrites) and power sources are inefficient at high frequencies. By contrast, the efficiencies for electro-optic phase shifting and harmonic generation increase with frequency, and devices based on these effects offer high-speed, low-loss operation over a wide spectral range.

20 DISTRIBUTION/AVAILABILITY OF ABSTRACT UNCLASSIFIED/UNLIMITED ☐ SAME AS RPT ☒ DTIC USERS ☐	21 ABSTRACT SECURITY CLASSIFICATION Unclassified
22a NAME OF RESPONSIBLE INDIVIDUAL M.B. Klein	22b TELEPHONE NUMBER (Include Area Code) (213) 317-5247 22c OFFICE SYMBOL

DD FORM 1473, 83 APR EDITION OF 1 JAN 73 IS OBSOLETE.

UNCLASSIFIED

SECURITY CLASSIFICATION OF THIS PAGE

Ferroelectrics are particularly promising for nonlinear and electro-optic applications at millimeter wavelengths, because their large linear polarizability leads to large electro-optic and nonlinear coefficients. The major challenge in developing ferroelectric materials for these applications is reduction of absorption losses. In this work we have evaluated and measured both intrinsic and extrinsic contributions in our samples, and have shown that the intrinsic factors dominate.

Perovskites were identified as the most promising class of materials, including $BaTiO_3$, $PbTiO_3$, $KNbO_3$, and $KTa_{1-x}Nb_xO_3$ (KTN). The material we chose to investigate is $BaTiO_3$, with a few mole percent $SrTiO_3$ added to stabilize the high temperature cubic phase. The resulting material, $Ba_{1-x}Sr_xTiO_3$ or BST, has properties which differ only slightly from $BaTiO_3$.

Major technical advances were as follows: (1) We have grown cm-sized single crystals of BST, the largest ever reported. These crystals were grown in 12 to 18 h, compared with 5 to 7 days for crystals grown by top-seeded solution growth. Future development of these crystals will address the elimination of inclusions, which at present restrict our ability to pole our crystals. (2) We have developed a convenient, accurate technique for measuring the dielectric constant and loss tangent of ferroelectric nonlinear materials, including $BaTiO_3$ and BST. The technique is based on the analysis of Fabry-Perot fringe patterns observed in transmission through samples mounted between the flanges of standard millimeter waveguides. We have measured the dielectric constant and loss tangent in $BaTiO_3$ at room temperature, and in BST for temperatures between 200 and 500°C. (3) We have made the first measurement of the linear electro-optic coefficient r_{33} in $BaTiO_3$ and the quadratic electro-optic coefficient g_{11} in KTN at millimeter wavelengths.

TABLE OF CONTENTS

LIST OF ILLUSTRATIONS

SECTION I

INTRODUCTION

Nonlinear materials offer great promise for use in devices such as phase shifters, modulators, switches, and frequency multipliers at frequencies above 50 GHz. State-of-the-art phase shifters (using ferrites) and power sources are inefficient at high frequencies. By contrast, the efficiencies for electro-optic phase shifting and harmonic generation increase with frequency, and devices based on these effects offer the promise of high-speed, low-loss operation over a wide spectral range.

One important reason for studying electro-optic and nonlinear materials at microwave frequencies is that the polarizabilities for certain materials (such as ferroelectrics) are much larger in the microwave region than in the visible. This enhancement is an important requirement since the efficiencies for phase shifting and harmonic generation decrease with wavelength and would otherwise be small in the near-millimeter spectral region. It has been shown that crystals with the largest microwave electro-optic (and nonlinear) coefficients are those with the largest values of linear susceptibility or dielectric constant. In the microwave region, the linear susceptibility can be much larger than that in the visible due to contributions from lattice vibrations. Ferroelectric materials are particularly known for their large dielectric constants at low frequencies, and are thus strong candidates for our consideration.

The major challenge in developing ferroelectric materials for nonlinear applications at millimeter wavelengths is reduction of absorption losses. The absorption coefficient or loss tangent in this spectral region has both intrinsic and extrinsic contributions. The intrinsic contribution is due to lattice absorption, and is largest in materials with the largest values of

dielectric constant. The extrinsic contribution is due to anion impurities, cation impurities, and possibly to domain wall motion. Our initial belief was that the millimeter-wave absorption in samples of interest is dominated by impurities. Measurements and analyses made during this program indicate the contrary; i.e. that the absorption is primarily intrinsic. This has led us to the study of the fundamental intrinsic millimeter-wave loss mechanisms in perovskite ferroelectrics, a technical area we hope to pursue in future programs with ONR.

Our initial survey of promising nonlinear materials resulted in the identification of perovskites as the most promising class of materials. Specific candidates include $BaTiO_3$, $PbTiO_3$, $KNbO_3$ and $KTa_{1-x}Nb_xO_3$(KTN). The specific material we chose to investigate is $BaTiO_3$, with a few mole percent $SrTiO_3$ added to stabilize the high temperature cubic phase. The resulting material, $Ba_{1-x}Sr_xTiO_3$ or BST, has properties which differ only slightly from $BaTiO_3$. The advantages and characteristics of BST are described more fully in Sections II and III.

During the course of this program several major technical advances were made. They are summarized very briefly below, and are described in greater detail in the following sections.

(1) We have succeeded in growing cm-size single crystals of BST, the largest to ever be reported. These crystals are grown in 12 to 18 hours, compared with 5 to 7 days for a similar size crystal of $BaTiO_3$ grown by the top-seeded solution growth (TSSG) technique. The major challenge in the development of these crystals is the elimination of inclusions, which at present restrict our ability to pole our crystals.

(2) We have developed a convenient, accurate technique for measuring the dielectric constant and loss tangent of ferro-electric nonlinear materials, including $BaTiO_3$ and BST. The technique is based on the analysis of Fabry-Perot fringe patterns observed in transmission through samples mounted between the flanges of standard millimeter waveguides. We have measured the dielectric constant and loss tangent in 4 commercial samples of $BaTiO_3$ at room temperature, as well as in two samples of BST for temperatures between 200°C and 500°C.

(3) We have made the first measurement of the linear electro-optic coefficient r_{33} in $BaTiO_3$ and the quadratic electro-optic coefficient g_{11} in KTN at millimeter wavelengths.

SECTION II

SELECTION OF MATERIALS

All common ferroelectric materials of interest for millimeter wave devices have crystal structures based on a network of oxygen octahedra. These octahedra can combine in space to form one of three common structures: perovskite, lithium niobate, and tungsten bronze. The advantage of octahedral-based compounds is that the structure is relatively open, and thus allows large ionic displacements in both the paraelectric and ferroelectric phases. Perovskite compounds (such as $BaTiO_3$, $SrTiO_3$, $PbTiO_3$, and $KNbO_3$) have the general formula, ABO_3, with the B cation having octahedral coordination, and the A cation having eight- to twelve-fold coordination. Lithium niobate compounds (such as $LiNbO_3$ and $LiTaO_3$) can also be expressed by the formula, ABO_3, with both A and B cations having octahedral coordination. In the perovskite and lithium niobate structures the transition from the paraelectric to ferroelectric phase is accompanied by shifts in the relative positions of the A and B cations with respect to the oxygen octahedral "cage" (and by slight realignment of the oxygen anions comprising the cage). One important characteristic of these structures is that all sites available to each of the two cations are filled, and the structures are translationally invariant or ordered. The tungsten-bronze ferroelectrics (such as SBN) have a more complicated structure, characterized by varying degrees of structural disorder (incomplete site filling or unknown site occupancy per unit cell).

Structural disorder in a material has two interrelated manifestations: (1) broadening of the ferroelectric phase transition (dielectric constant versus temperature); and (2) introduction of dielectric relaxation in the frequency spectrum, especially for $T<T_c$. These two effects arise from the interaction of the soft mode with structural fluctuations. Broadening

of the phase transition results from increased damping of the soft mode, and produces increased loss at all frequencies. Dielectric relaxation reduces the dielectric constant and further increases the loss at high frequencies.

We have chosen to concentrate our interest on perovskite materials, primarily because of their ordered crystal structure. There are a variety of promising materials in this structural class, including many with large values of dielectric constant and large calculated values of millimeter wave nonlinear coefficients. Furthermore, most perovskites are single component materials and are thus easier to grow than the tungsten bronzes, which are mixed composition materials and are thus subject to compositional variations (e.g., striations).

Among the perovskites, we have chosen $BaTiO_3$ for several reasons: (1) its millimeter-wave nonlinear coefficient (measured via frequency mixing at 58 GHz[1]) is known to be large, (2) preliminary measurements have indicated that high purity samples could be obtained using reactive atmosphere processing (RAP), (3) it presents fewer growth problems than $PbTiO_3$ (high PbO loss) and fewer poling problems than $KNbO_3$ (orthorhombic at room temperature), and (4) it has many promising applications in the visible spectral region.

The modification of $BaTiO_3$ through the introduction of several mole percent $SrTiO_3$, as done for this program, has little impact on the basic materials parameters. In Table 1, the fundamental properties of both systems are compared, based on literature data. Although the mixed crystals have not yet been fully characterized, it is clear that the structural, dielectric and piezoelectric properties of both systems are very similar. Therefore, approximately the same high values for the electro-optic coefficients can be expected for $Ba_{1-x}Sr_xTiO_3$. The linear and nonlinear optical properties, at millimeter as well as visible wavelengths, will be comparable in both systems.

Table 1. Properties of $BaTiO_3$ and $Ba_{1-x}Sr_xTiO_3$

15253-13

PROPERTIES		$BaTiO_3$	$Ba_{1-x}Sr_xTiO_3$	UNITS
Sr CONCENTRATION		–	x = 0.03	
TRANSITION TEMP.	T_c	131-134	114	(^oC)
LATTICE PARAM. (AT 20^oC)	a	3.9920	3.989	(Å)
	c	4.0361	4.032	(Å)
MAX. DIELECTRIC CST.		7800	15000	
CURIE CONSTANT		180,000	210,000	(^oC)
CURIE-WEISS TEMP.		112	99	(^oC)
DELECTRIC CST. (AT 20^oC)	ϵ_a	3700	4300	
	ϵ_c	135	600 (*)	
SPONT. POLARIZATION	P_s	0.25	0.12 (*)	(C/m^2)
COERCIVE FIELD	E_c	100	240 (*)	(kV/m)
PYROEL. COEFF.	P	$2x10^{-8}$		($C\ cm^{-2}\ K^{-1}$)

(*) POLYDOMAIN CRYSTALS.

REFERENCES:

LANDOLT-BORNSTEIN GROUP III, VOL. 16, FERROELECTRIC OXIDES.

M.E. LINES AND A.M. GLASS, PRINCIPLES AND APPLICATIONS OF FERROELECTRICS AND RELATED MATERIALS, CLARENDON, OXFORD (1977).

I. CAMLIBEL, M. DiDOMENICO AND S.H. WEMPLE, J. PHYS. CHEM. SOLIDS 31, 1419 (1970).

S. UEDA, MAT. RES. BULL. 9, 469 (1974).

SECTION III

GROWTH AND PROCESSING OF $Ba_{1-x}Sr_xTiO_3$

A. INTRODUCTION

Barium titanate occurs in five crystalline forms. With increasing temperature, the stable phases are rhombohedral, orthorhombic, tetragonal, cubic and hexagonal. It is the tetragonal phase that is stable at room temperature and which is of primary interest for its nonlinear properties. The transformation between the cubic and hexagonal phases is reconstructive in nature, whereas all the other transitions are displacive. Consequently, hexagonal $BaTiO_3$ cannot be converted to the cubic form without destroying the optical quality of the crystal. It is therefore necessary when designing a crystal growth technique for this material to avoid the high temperature hexagonal phase that normally crystallizes from the melt at ~1620°C.

One successful approach to this problem was developed by Linz and coworkers[27] and involves growth from solution in the system $BaTiO_3$-TiO_2. Crystals commercially available from Sanders Associates have been grown in this fashion. In such an approach, growth takes place at temperatures within the stability range of cubic $BaTiO_3$. The principal disadvantage of the technique is that it is slow, requiring a minimum of 5 to 7 days for the growth of an appreciable sized crystal.

An alternative approach derives from the fact that the cubic-hexagonal transition temperature is very sensitive to impurities. Substitution, for example, of small amounts of Sr or Ca for Ba results in the complete elimination of any stability field for hexagonal $BaTiO_3$. Thus, the desired cubic phase can be grown directly from melts in this system. Of course, the resulting crystals are solid solutions but, as was discussed above, small additions of a solute such as $SrTiO_3$ should not greatly alter the crystalline properties from those of pure $BaTiO_3$.

SECTION IV

MEASUREMENT OF LINEAR DIELECTRIC PROPERTIES

A. DESCRIPTION OF TECHNIQUE

In measurement of dielectric constant and loss tangent in our samples, we drew on our experience at Hughes Research Laboratories with techniques making use of the Fabry-Perot properties of plane-parallel samples. The plane-wave transmission through such samples yields characteristic fringes as a function of frequency or temperature (see Appendix A); the free spectral range yields the dielectric constant or refractive index, and the contrast or peak transmission yields the loss tangent or absorption coefficient.

Using the above technique, we had measured ϵ and tan δ in $LiNbO_3$ and $LiTaO_3$ at 94 GHz using samples mounted in free space between transmitting and receiving horns.[7] In this experiment, sample mounting was convenient, but large samples were required to avoid diffraction effects. In a separate experiment,[8] we measured ϵ and tan δ in KRS-5, TlBr, teflon and rexolite at 94 GHz using samples mounted inside conventional hollow metal waveguide. For this mounting configuration the required sample size is considerably reduced, but mechanical tolerances are restrictive. In order to achieve tight fit of the above samples within the waveguide, the materials were actually pressed into place. This cannot be done for the hard samples of interest to this program.

In the past year we have developed a mounting technique which takes the best properties of each of the techniques described above. Our samples are mounted between the flanges of two standard rectangular metal waveguides. In this configuration, the samples can be nearly as small as the waveguide cross section, but they do not need to be fitted within the waveguide. We have measured a large number of materials with this

walls which are parallel to pseudo-cubic {110} planes, whereas 180° domains have boundaries with "wavy" shapes. Both types of domains have to be eliminated in order to obtain a useful electro-optical crystal. For dielectric constant measurements alone, it is sufficient to get rid of the 90° domains only.

In order to actually perform the poling of a $BaTiO_3$ or BST crystal, one can adjust three parameters, namely, the temperature, electric field and uniaxial pressure, all three of which have an impact on the domain structure. Increasing the temperature increases the mobility of the domain walls, applying an electric field partially aligns the polarizations, and applying pressure favors certain domain configurations. We have found that it is possible to achieve poling by first removing the 90° domains and then removing the 180° domains in two separate processing steps. Mechanical poling, which itself consists of one or more steps where uniaxial pressure is applied to the crystal, will result in a state where the direction of the tetragonal axis is perfectly determined but with a sign ambiguity. Electrical poling will then determine the sign of the polarization. Our mechanical poling technique is similar to the procedure used by Sanders Associates to pole their $BaTiO_3$ crystals. However, every crystal is a special case and the number of steps needed to achieve a single domain state is large and difficult to predict a priori. The "easiest" crystal to pole so far required four different mechanical steps and one electrical poling step. Moreover, crystals with minor imperfections have proven to be difficult to pole because imperfections act as pinning points for the domain walls. We have poled high quality commercial $BaTiO_3$ crystals which had been heated above T_c, but we have not been able until now to obtain a truly single domain BST crystal. Our present BST crystals have too many inclusions and inhomogeneities. Under pressure, the domains walls will vanish and, in the stressed state, a crystal free of 90° domains can be obtained. Upon releasing the pressure, however, some domains will reappear in order to accomodate the zero-pressure random strains generated by the imperfections. A slight improvement in the crystal quality should solve this problem.

15253-2

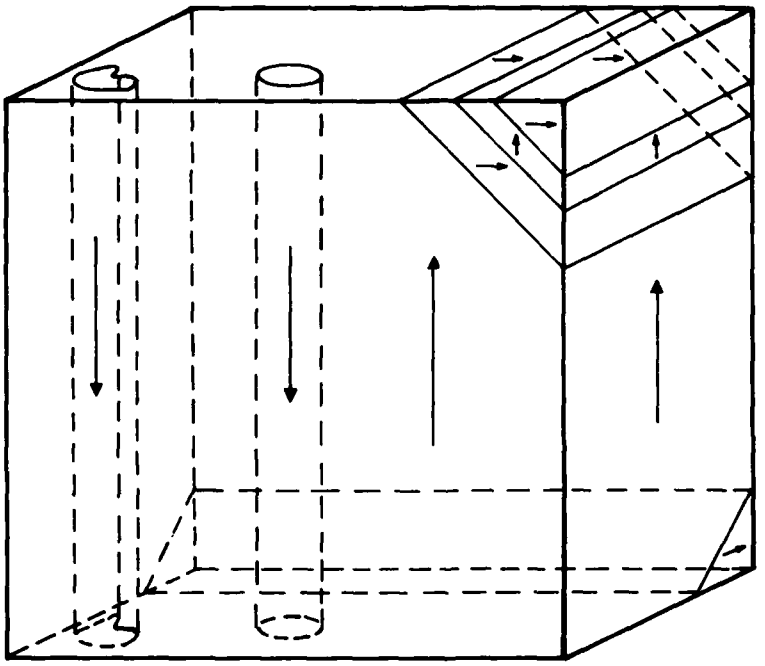

Figure 6. Domain structure of $BaTiO_3$ in tetragonal phase. The arrows represent the direction of polarization.

from the crystals. Of course, these results do not preclude the possibility that similar atmospheres may be effective, when applied during growth, in preventing OH^- from entering the crystals.

All the crystals, iron-doped or nominally undoped, are yellow in color. Annealing in nitrogen for 24 hours at 800°C makes their coloration lighter. Annealing also apparently relieves some internal stress in the crystals, thereby promoting domain wall mobility. This is beneficial for the poling process.

E. POLING

On cooling $BaTiO_3$ or BST crystals from the cubic (paraelectric) phase to the tetragonal (ferroelectric) phase, there are six equivalent directions (i.e., the <100> axes of the cubic phase) along which the spontaneous polarization may occur. Different regions of the crystals polarize in each of these directions, each volume of uniform polarization being referred to as a domain. In an as-grown crystal and in the absence of an electric field, the multidomain state which appears upon cooling prevents any net polarization. Therefore, such crystals show very small, if any, piezoelectric, pyroelectric and electro-optic effects. These effects depend on the sign of the polarization and are thus averaged out to zero in a multidomain crystal. For this reason, it is important to find a procedure (called poling) leading to a single domain state.

The domain structure of $BaTiO_3$ and BST is schematically shown in Figure 6. Two types of domains are observed: domains whose polarizations lie at 90° to each other and domains with antiparallel polarizations. The so-called 90° domains are readily seen when the crystal is put between crossed polarizers. The 180° domains are more elusive: we have been able to observe them on as-grown and on polished surfaces which had been etched in HF or in HCl. It should be noted that 90° domains are separated by

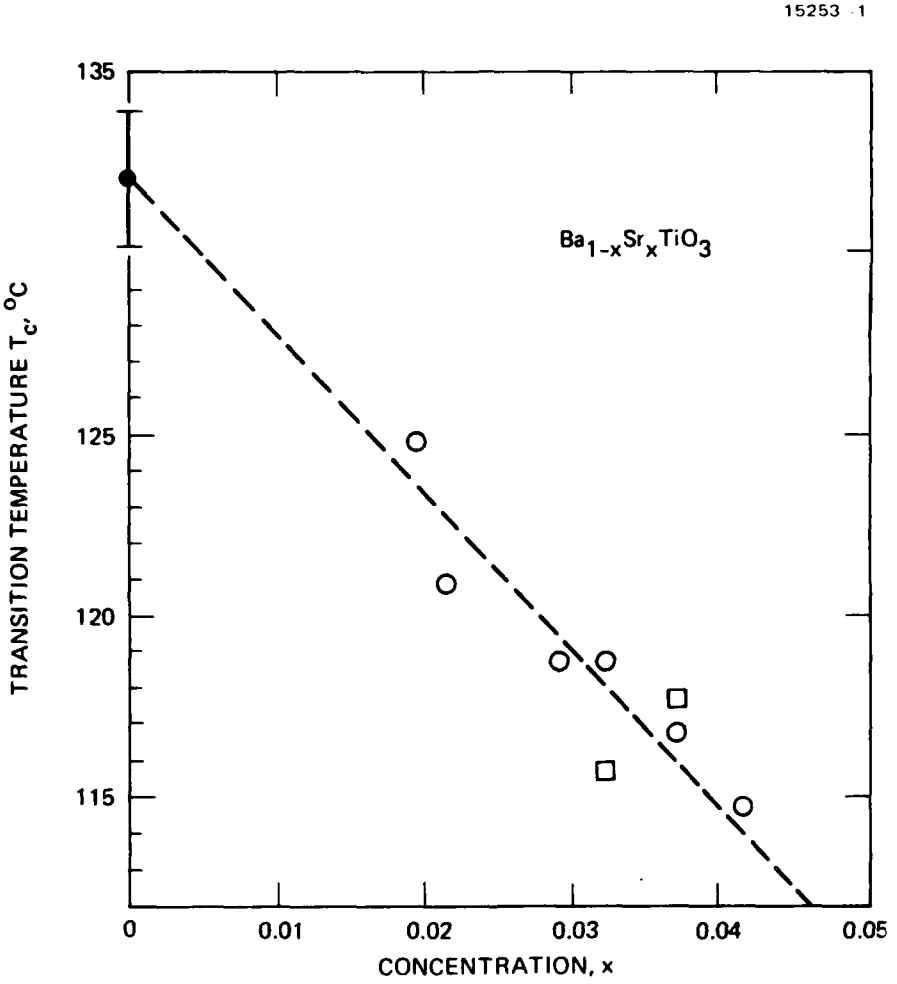

Figure 5. Concentration dependence of the transition temperature. Circles indicate crystals grown from high purity starting materials, squares indicate standard purity starting materials.

The Sr concentration has also been determined and was found to be always slightly higher in the crystals than in the melt. This is not in agreement with the presumed existence of a congruent melting composition. The reason for this discrepancy is not understood. The corresponding paraelectric-to-ferroelectric transition temperatures T_c have been measured by differential scanning calorimetry (DSC). As expected, T_c decreases with increasing x. The experimental results are displayed in Figure 5. The following empirical law is obtained in the concentration range presently investigated :

$$T_c\ (°C) = 132 - 440\ x.$$

Our crystals have transition temperatures in the range between 115 and 125°C.

D. POST-GROWTH TREATMENT

One of the original goals of this work was to carry out growth under a reactive atmosphere in order to produce OH^- - free crystals. Unfortunately, this proved impractical for the growth apparatus that was available. As an alternative, we investigated the possibility of removing the OH^- impurity from our crystals through post-growth processing. Polished crystals of 3 to 4 mm on an edge were heated in a sealed horizontal tube furnace. Flowing atmospheres of either N_2, $CO/CO_2/I_2$, or O_2/Br_2 were maintained during heating to between 700 and 1000°C, with processing times of ~24 hours.

Infrared spectra obtained on a Bomem FTIR clearly show the presence of absorption bands near 3500 cm^{-1} in the as-grown crystals, corresponding to the O-H stretching mode. Although it was not always possible to compare the spectra of one crystal both before and after RAP treatment, it is nevertheless apparent that none of the treatments was successful in eliminating OH^-

Table 2. Impurities in $Ba_{1-x}Sr_xTiO_3$ Single Crystals

15253-12

	SIMS	EMISSION SPECTROGRAPHIC ANALYSIS		S. UEDA
		ppm	ppm	(1974)
H	*			
C	*			
Na	*	430	<1000	<400
Mg	*		20	<10
Al	**	160	<10	<100
Si	**	350	<250	<10
Cl	o			
K	*	220	<18000	<20
Ca	*	200	350	<100
Cr	o			
Mn	*			
Fe	o	80	<80	<100
Ni	*			
Cu	o			<10
Mo		<15	<50	
Pt	**	120	<100	
Bi		TR		

** MAJOR IMPURITY
* IMPURITY
o TRACES TR TRACES

These experiments demonstrate the feasibility of Czochralski growth of BST in a fast and reproducible way. Due to the small size of the furnace, which dictated the use of small crucibles, the thermal and hydrodynamic instabilities will be relatively large. Upscaling the process would undoubtedly result in high quality crystals and lead to considerable improvements in the poling process (see Section E. below).

C. CHARACTERIZATION

The Sr concentration and the impurity content of the BST crystals were checked with various techniques. First, Secondary Ion Mass Spectroscopy (SIMS) provided a qualitative analysis of the impurities present in the crystals. The major impurities, according to this technique, turned out to be Pt, whose source is, of course, the crucible material, and Al and Si, which stem from the refractories in the furnace. The Fe content of an intentionally doped crystal appeared to be approximately five times higher than in a nominally undoped crystal. A more quantitative analysis was provided by atomic absorption and emission spectroscopy. Table 2 provides an overview of the results. The overall agreement between the different techniques is satisfactory when taking into account their respective detection limits (with the exception of Al, where not even order of magnitude agreement is achieved). It should be noted that no Mo has been detected, although the presence of this element could be suspected due to the nature of the heating elements. The rather high level of platinum incorporated into the BST crystals is a drawback of the very high growth temperature (with respect to the melting point of platinum) leading to a high solubility of the crucible material in the melt. Previous growth experiments of BST reported in the literature[3,4] have been performed with iridium or rhodium crucibles and spectroscopic analysis[4] revealed the presence of 0.02 wt% Ir and 0.26 wt% Rh. Our level of Pt contamination nevertheless compares favorably with the figure reported for "butterfly wings"-type $BaTiO_3$ crystals where a concentration of 0.10% of Pt has been reported.[5,6]

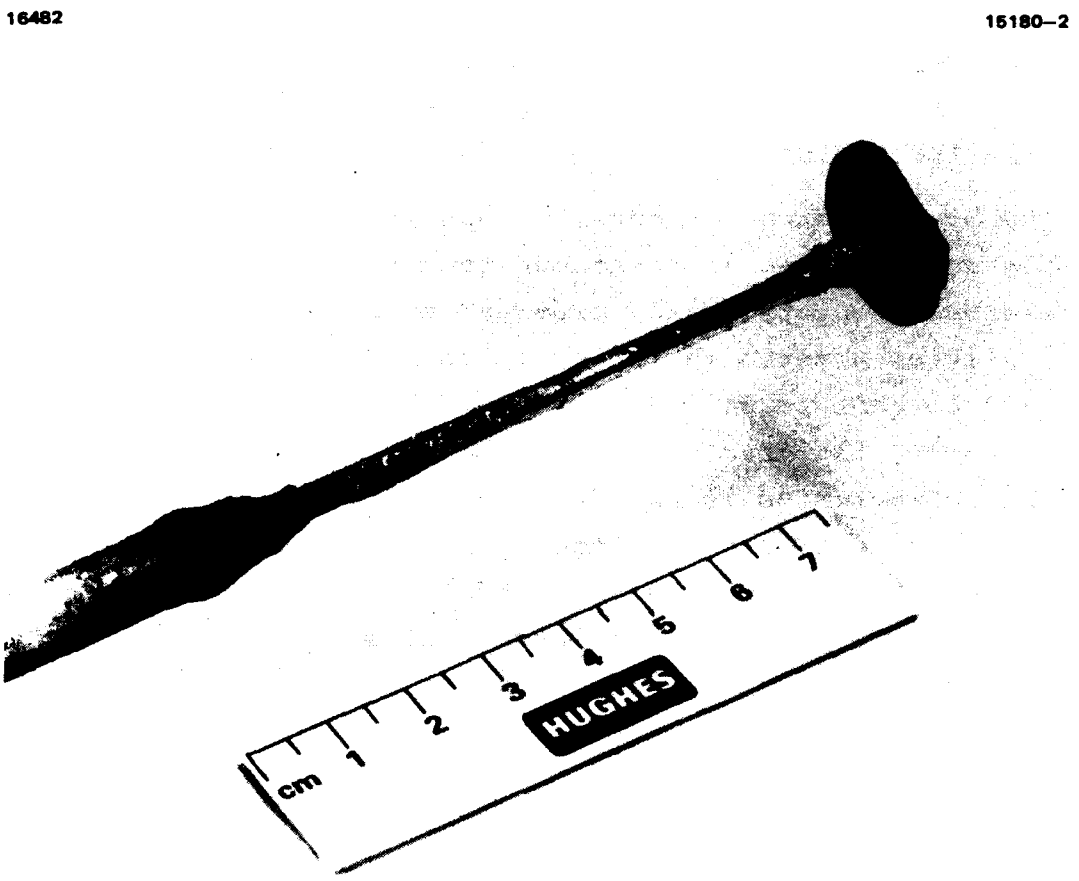

Figure 4. $Ba_{1-x}Sr_xTiO_3$ (x=0.035) crystal grown on a (100) seed.

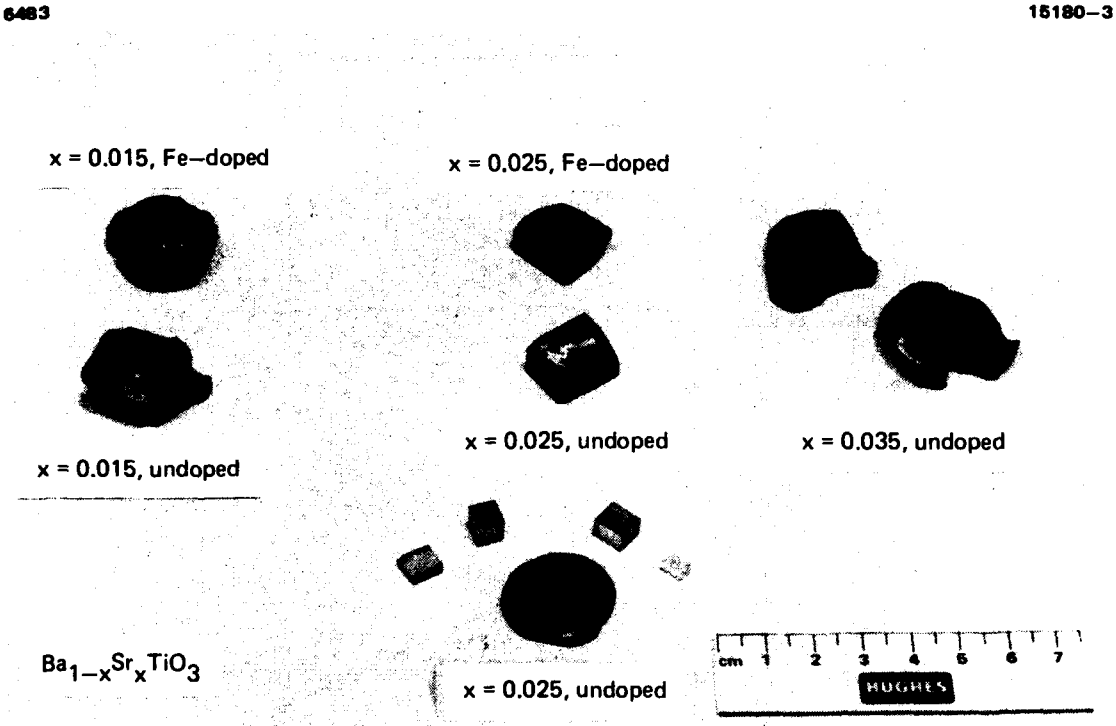

Figure 3. $Ba_{1-x}Sr_xTiO_3$ crystals grown by spontaneous nucleation on a platinum rod.

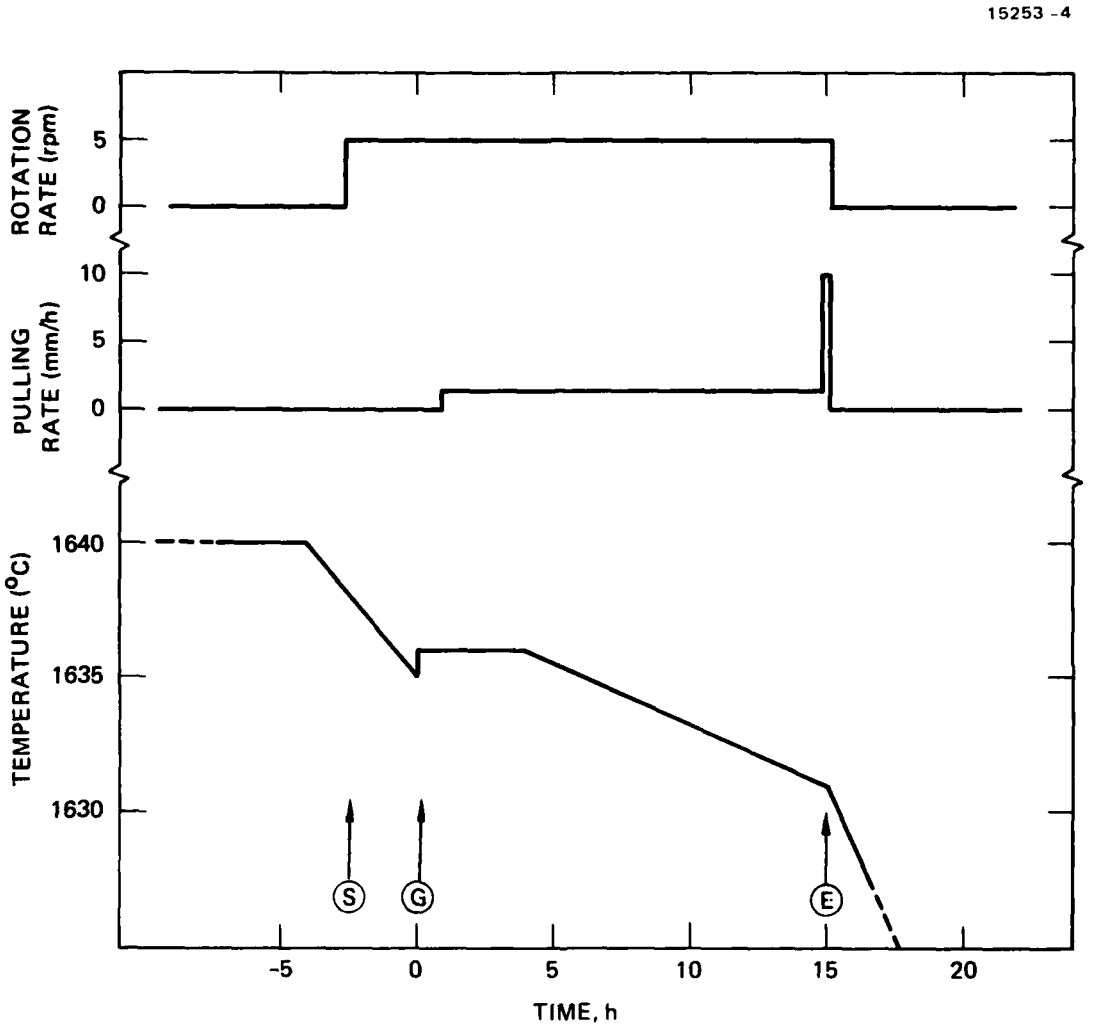

Figure 2. Parameters for growth of $Ba_{0.975}Sr_{0.025}TiO_3$ as a function of time. The symbols indicate the seed is in contact with the melt (S), growth starts (G), and when the crystal is withdrawn from the melt (E).

starting chemicals. Crystals were grown from melts varying in composition from 1.5 to 3.5 mol% $SrTiO_3$. Usually, melts were replenished after each run so that additional crystals could be grown from the same melt. In several cases, Fe-doping was attempted in order to evaluate its effect on the crystal growth and material properties. This was accomplished by adding Fe_2O_3 to the melt at a level of 100 to 200 ppm atomic.

In a first series of runs, unseeded growth was carried out using a long platinum rod as a nucleation point. The rod acted as a heat sink. As depicted in Figure 1, the platinum rod was attached to an alumina tube which was connected to the pulling mechanism. The charge was melted at about 1650°C for 15 hours and then slowly cooled to the nucleation temperature, with the rod touching the melt and rotating at 7 rpm. When the nucleus reached the proper size, the temperature was raised by about 2°C and pulling at a rate of 0.6 mm/h was inititated. Approximately three hours after nucleation, a temperature program was started at a rate of -0.5°C/h for about 15 hours. When the final temperature was reached, the crystal was pulled out of the melt and allowed to cool at -1°C/h to 1600°C, -10°C/h to 1500°C and at -40°C/h to room temperature (in an afterheater for temperatures below 800°C). The evolution with time of all these growth parameters is summarized in Figure 2. Such experiments yielded crystals with a small number of grains or even single crystals. The growth direction was most frequently <100>, but occasionally <110> and <111> directions were also observed. Crystals as large as $20 \times 20 \times 8$ mm^3, weighing up to 20 grams, could be obtained (see Figure 3) despite the small crucible volume.

In a second series of runs, seeds with (100) faces were attached with platinum wires to the platinum rod. The growth parameters were the same as mentioned previously for the unseeded runs. Once the nucleation temperature had been determined in an unseeded run, immersing the seed resulted in a perfectly square nucleus which would produce a single crystal (see Figure 4). The quality of the crystals increased markedly when good seeds became available.

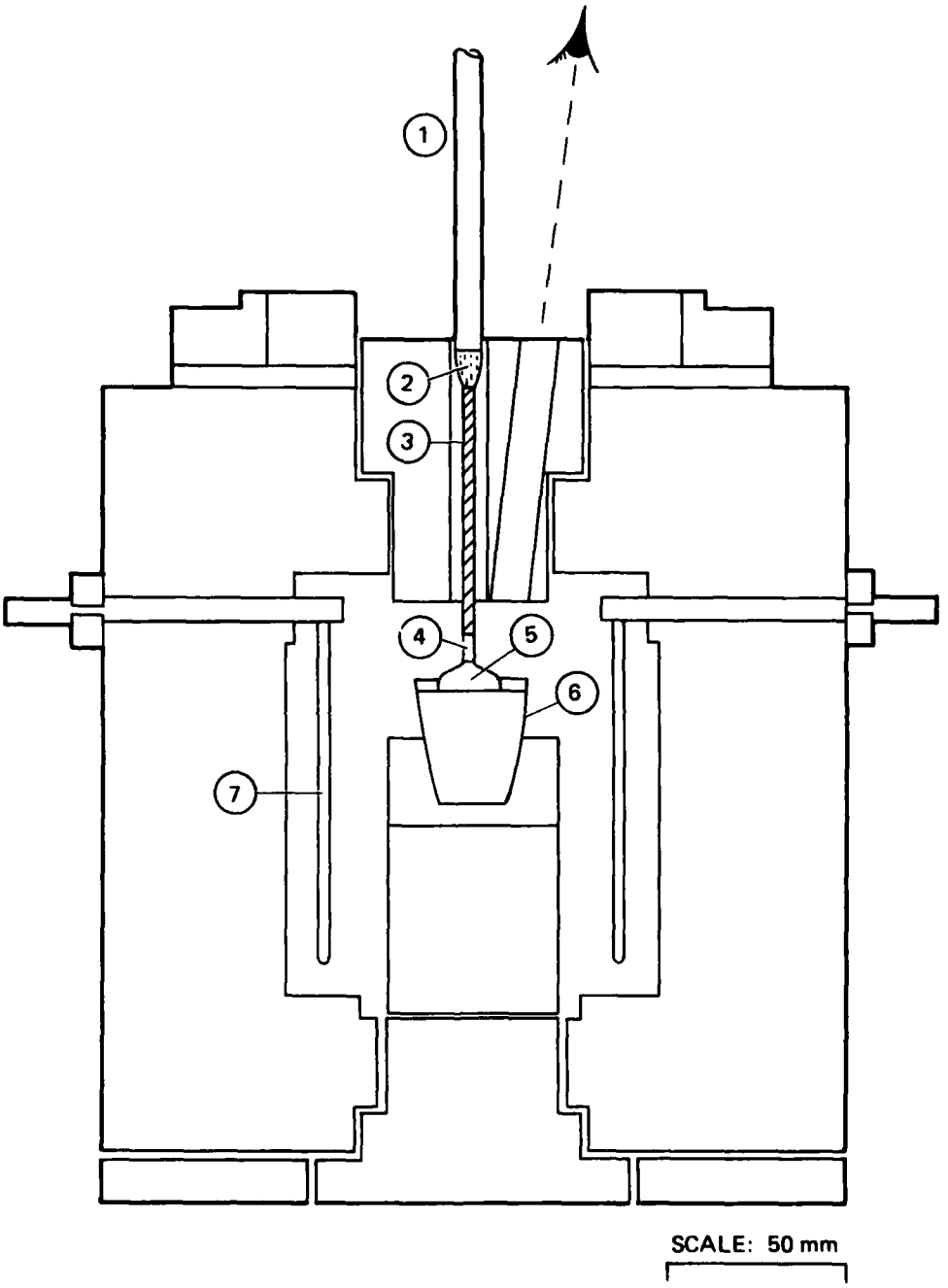

Figure 1. Experimental setup for Czochralski growth of $Ba_{1-x}Sr_xTiO_3$. Note the scale of the furnace chamber. Symbols refer to (1) alumina pullrod, (2) high temperature cement, (3) platinum rod, (4) seed, (5) growing crystal, (6) platinum crucible, and (7) $MoSi_2$ heating element.

The phase diagram of the system $BaTiO_3$-$SrTiO_3$ was studied by Basmajian and DeVries.[2] According to their results, the addition of Sr stabilizes the cubic phase to the melting point when the concentration x = [Sr]/{[Sr] + [Ba]} is greater than 0.012. Moreover, the suggested presence of a melting minimum in this system near x = 0.025 provides an appropriate composition from which Czochralski growth should be possible. The Czochralski method has a number of inherent advantages over other methods. For example, the duration of a growth run is typically less than a day, as compared with the week that is required for top seeded solution growth. Unfortunately, the phase diagram is not known with sufficient certainty to pinpoint exactly the value of x for which congruent melting occurs. It is therefore necessary to determine empirically the best melt composition over a range of x values from which to pull crystals.

B. CRYSTAL GROWTH EXPERIMENTS

Growth experiments took place in a commercial 1.5 kW, resistively heated furnace. Molybdenum disilicide (Kanthal Super) heating elements were used in a cylindrical configuration. A drawing of the furnace can be found in Figure 1. The furnace chamber (Ø 40 x 100 mm) could accomodate a 30 cm^3 platinum crucible supported by a molded high-temperature ceramic holder atop a pedestal. The height of the pedestal could be adjusted in order to obtain the proper temperature gradient at the melt surface.

Melts were prepared from mixes of commercial $BaTiO_3$ and $SrTiO_3$ powders, with crucibles containing between 70 and 100 grams of melt per run. Starting powders were obtained from a variety of sources, but the use of purer materials consistently resulted in the presence of fewer inclusions and better overall crystal quality. Except where noted, the crystals described in this report were grown with Johnson Matthey Puratronic (Grade 1)

technique (see Appendix A) and have found it to be convenient and reliable. All dielectric measurements at fixed temperature were performed at UCLA, and all measurements at fixed frequency were performed at Hughes.

B. EXPERIMENTAL RESULTS

The fundamental material of interest to this program is $BaTiO_3$, either in its undoped form, or Sr-doped (i.e., BST). Since commercial undoped samples of $BaTiO_3$ were available from other programs at Hughes, we began our characterization efforts by measuring the linear properties of these samples. In each case, the sample as delivered by the supplier (Sanders Associates) was free of 90° domains. The removal of 180° domains was achieved by heating the crystals to 125° to 130°C, applying a few kV/cm, and cooling slowly to room temperature.

In our experiments the samples were oriented to measure $\epsilon_c = \epsilon_{33}$, the dielectric constant for fields polarized along the c-axis. In Table 3 we present a summary of our measurements performed at room temperature in the range 60 to 75 GHz. We note that two samples had $\epsilon_c \simeq 58$ and two had $\epsilon_c \simeq 55$ and attribute this difference to systematic or calibration errors, not to a fundamental difference in the dielectric properties. We were also unable to detect any dispersion in ϵ across the indicated frequency range. We have chosen

$$\epsilon_c = 57$$

as an average value, with a ±3% spread among the samples. The corresponding value of refractive index is

$$n = 7.5.$$

Table 3. Linear Dielectric Parameters of $BaTiO_3$ in the Millimeter Spectral Region. The Microwave Electric Field is Polarized Along the C-Axis of the Crystal

15253-8

$BaTiO_3$ SAMPLE	REFRACTIVE INDEX n	DIELECTRIC CONSTANT ϵc	MEASUREMENT FREQUENCY (GHz)	ABSORPTION COEFFICIENT α (cm^{-1})	LOSS TANGENT TAN δ	APPEARANCE
R2	7.67	58.8	75	2.9	0.024	CLEAR
GB4	7.65	58.5	60	2.1	0.022	CLEAR
			75	2.9	0.024	
BW1	7.40	54.8	60	1.9	0.021	DARK
			75	2.6	0.023	
BS1F	7.43	55.2	60	2.3	0.024	LIGHTLY COLORED
			75	2.8	0.024	

The average value of the loss tangent across the range 60 to 75 GHz is

$$\tan \delta \simeq 0.024,$$

with a ±10% spread among the samples. The loss tangent is expected tc increase with frequency (see Equation (1) below), but any such variation is masked by the spread of experimental values.

In the last column of Table 3 we have noted the appearance of each crystal. In general, darker samples correspond to higher concentration of cations, especially transition metal impurities. The insensitivity of the loss tangent values to the cation impurity concentration suggests that these spe es do not cause extrinsic millimeter-wave losses. It should be noted that the crystal color indicates nothing regarding anion impurities (OH^-, etc.).

In Table 4 we have summarized values of ϵ_c measured above piezoelectric resonances at room temperature in solution-grown single-domain crystals of $BaTiO_3$. At low frequencies, values of 60 and of 80 are reported. At higher frequencies, a small drop in ϵ_c is observed,[21] presumably due to clamping of domain wall motion. At 56 GHz, a value ϵ_c=57 was reported,[1] in excellent agreement with our result. Finally, the Raman value of 31 is the limit at frequencies approaching the TO mode frequencies. The dispersive properties of ϵ_c at these very high frequencies are not well understood, and have never been directly observed; the study of this behavior is one part of our proposed follow-on effort.

Table 4. Dielectric Constant at Room Temperature for Single Crystal $BaTiO_3$

15253-14

FREQUENCY	ϵ_c	REFERENCE
75 MHz	60	9
250 MHz	80	10
6 GHz	53	21
56 GHz	57	1
60-75 GHz	57	THIS WORK
RAMAN	31	22

The only reported loss measurement in solution-grown $BaTiO_3$ at millimeter wavelengths is a value of α=1.7 cm^{-1} at 56 GHz,[1] with no information given as to how the measurement was made. At this same frequency our measured value of loss tangent corresponds to α=2.1 cm^{-1}, which is in good agreement with Ref. 1, considering the unknown accuracy of the earlier measurement.

As mentioned earlier, our samples of BST grown at Hughes cannot be characterized at room temperature until we are able to remove all 90° domains. In the meantime we have been able to characterize these samples at temperatures above the ferroelectric transition temperature, T_c, where the material is cubic, and thus has no domains. These measurements are described in Appendix B. Although relatively large losses limit the experimental accuracy, we find reasonably good agreement with other measurements in undoped $BaTiO_3$.

C. LOSS MECHANISMS IN $BaTiO_3$

In order to evaluate the usefulness of a candidate nonlinear material for practical devices, it is important to understand and evaluate the losses in a given frequency band. As mentioned earlier, the loss tangent has both intrinsic and extrinsic contributions. If one could show that extrinsic factors contribute significantly to the measured loss, then one might hope that the control and elimination of these factors would lead to a substantial reduction in the loss tangent, and thus improvement in the device performance.

For the particular case of $BaTiO_3$, our initial belief was that the absorption was dominated by impurities. This was based on our calculated value of loss tangent, which was two orders of magnitude smaller than the measured value in the literature. On this basis, we felt that RAP processing to remove impurities was a promising approach to producing low-loss $BaTiO_3$. As a result of our measurements and analysis to be described below, we now believe that the absorption in our solution-grown crystals is primarily intrinsic.

The major factor contributing to the intrinsic loss at high frequencies is lattice absorption; i.e., the interaction with TA and TO phonons. There are several different phonon interactions which can contribute to the losses, as shown schematically in Figure 7. The wave vector diagram[23] is for the strongest TA and TO mode in $BaTiO_3$, with the electric field polarized along the c-axis--the so-called A-modes. Interaction (a) is the fundamental zone-center TO-mode absorption which is most commonly considered in ionic solids. A phenomenological harmonic oscillator model[11] for this case gives

$$\tan \delta = \gamma\omega/\omega_o^2, \qquad (1)$$

where γ is the damping coefficient, ω_o is the mode frequency, and ω is the frequency of interest. The sources of the damping are not specified in this model; ω_o and γ must be measured independently. Physically, the mechanism leading to damping is thought to be anharmonicity in the ion potential,[24] leading to coupling to higher order modes, and eventually to heating of the crystal.

In $BaTiO_3$, several measurements of γ and ω_o exist for the conditions of interest. Typical values[25,26] are ω_o=178 cm^{-1} and γ=3 cm^{-1}. At 60 GHz, the corresponding value of loss tangent is $\tan \delta = 2 \times 10^{-4}$. It was on the basis of this low value that we felt that the higher measured value of loss tangent must include a large extrinsic contribution.

During the course of this program we became aware of another intrinsic phonon loss contribution: multi-phonon absorption, represented by (b) and (c) in Figure 7. These contributions are especially important for frequencies that are much smaller than the lattice frequency, ω_o, as is true in our case. Interactions (b) and (c), consisting of the destruction of a TA phonon and the generation of a TO phonon, are known to contribute the dominant portion of the losses at microwave frequencies in the alkali halides.[24] Interaction (c) is expected to be especially

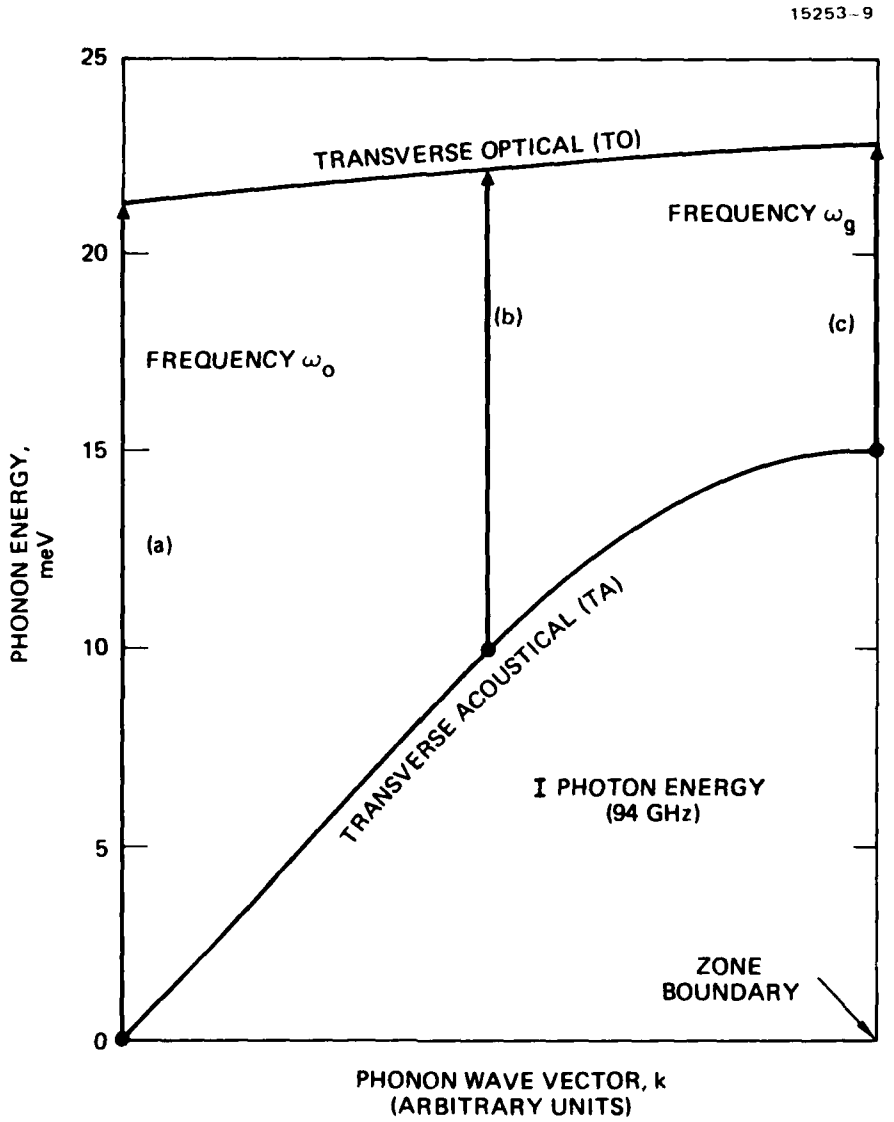

Figure 7. Phonon dispersion diagram for lowest-order TA and TO modes in $BaTiO_3$ with $\vec{E} \parallel \vec{c}$.[23] Also shown are allowed optical transitions: (a) zone center, (b) two-phonon, arbitrary k, and (c) two-phonon zone boundary.

large, because the resonance frequency, ω_g (corresponding to the forbidden "gap"), is much closer to ω than is the TO mode frequency, ω_o. This more than compensates for the limited population of TA phonons at room temperature.

An accurate calculation of the loss tangent in $BaTiO_3$ based on multi-phonon absorption is beyond the scope of this program, but is part of a proposed follow-on effort. However, from our examinations of the literature we now believe that the combined effects of all intrinsic loss mechanisms should lead to a value of loss tangent consistent with our measured value. We do not rule out the possibility that anion impurities (e.g., OH^-) may still play a role, but probably not a major one. Some references also suggest that domain wall motion may contribute to the losses,[21] but we see no evidence of this in our samples.

SECTION V

PHASE SHIFTING IN KTN AND $BaTiO_3$ AT 94 GHz

In our work preceeding the present program we developed scaling laws which indicate the strong dependence of the electro-optic coefficient on the linear refractive index, or dielectric constant.[7,11,13] The induced electro-optic phase shift may be written as

$$\Gamma = (2\pi L/\lambda)\ \Delta n = \begin{cases} \pi L/\lambda\ n^3 r\ E & \text{(linear effect)} \\ \pi L/\lambda\ n^3 g\ P^2 & \text{(quadratic effect)}, \end{cases} \tag{2}$$

where L is the interaction length, λ is the free-space wavelength, n is the refractive index, r is the linear electro-optic coefficient, E is the applied modulating field, g is the quadratic polarization-optic coefficient, and P is the induced polarization due to the modulating field, E ($P=\epsilon E$). Thus, the effective electro-optic coefficient (containing all material properties) for the linear effect is $n^3 r$, and the effective coefficient for the quadratic effect is $n^3 \epsilon^2 g$, or $n^7 g$. It was shown[11,13] that the effective coefficients scale as

$$n^3 r \sim n^5 \sim \epsilon^{5/2}$$

and

$$n^7 g \sim n^7 \sim \epsilon^{7/2}.$$

This clearly demonstrates the strong variation of the electro-optic coefficients with n and ϵ. In absorbing materials a different figure of merit is appropriate, as will be described in Section VI.

Before the start of the present program, we had measured effective electro-optic coefficients in $LiNbO_3$ and $LiTaO_3$ at 94 GHz, using a measurement technique developed at Hughes.[7] The key feature of this technique was the insertion of the sample in

one arm of a balanced bridge, thereby converting the electro-optic phase shift into amplitude modulation. The samples were mounted in free space between transmitting and receiving horns, and quarter-wave matching plates were attached to the input and output crystal faces to reduce Fresnel reflections.

In the work reported here, we have used the same bridge technique (see Figure 8) to measure electro-optic coefficients in $BaTiO_3$ and KTN. The $BaTiO_3$ was a poled sample from Sanders Associates, and the KTN, provided by D. Rytz, had a composition expressed as $KTa_{0.91}Nb_{0.09}O_3$. This material has a Curie temperature of 95 K and is thus cubic at room temperature. The resultant electro-optic effect in this material is quadratic.

For our measurements the crystal samples were mounted between waveguide flanges in a manner similar to that used to measure the dielectric properties (see Figure 9). In order to reduce Fresnel reflections at the sample surfaces, we used quarter-wave plates as shown. The materials for the quarter-wave plates were BaF_2 (for the $BaTiO_3$) and GaAs (for the KTN). We also included a thin kapton sheet adjacent to each flange, to prevent arcing from the electrodes to the flanges. Although the kapton does eliminate the arcing, the close proximity of the flanges to the electrical contacts results in a nonuniform electric field distribution in the electro-optic samples. While we have not calculated the exact field distribution, we believe that the perturbation from the flanges is not a large effect. If necessary, the perturbation could be reduced by adding thicker dielectric layers between the sample and the flanges in a way which maintains the low reflectivity of the structure.

The bridge shown in Figure 8 was first balanced by adjusting the variable attenuator for maximum fringe contrast. The adjustable phase shifter was then set at the midpoint of the fringe pattern, i.e., in the linear region. For this bias condition an ac voltage applied to the crystal causes an amplitude variation on the detector at the applied frequency (for the case of a

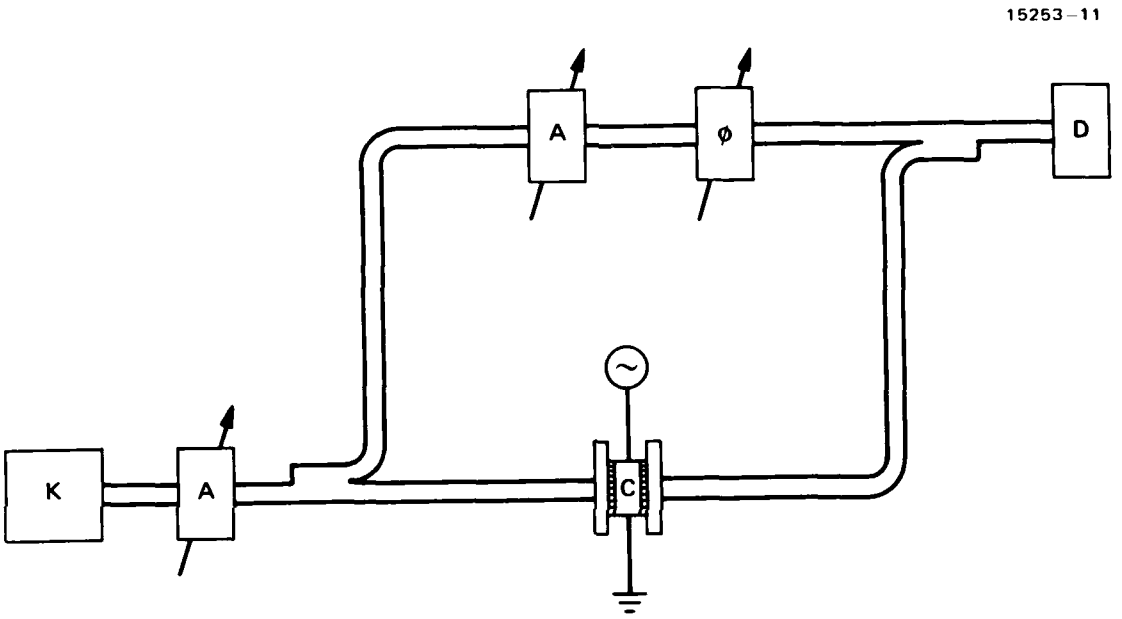

Figure 8. Bridge arrangement for measurement of electro-optic phase shifts. K = klystron, A = variable attenuator, ϕ = variable phase shifter, C = sample crystal and D = detector.

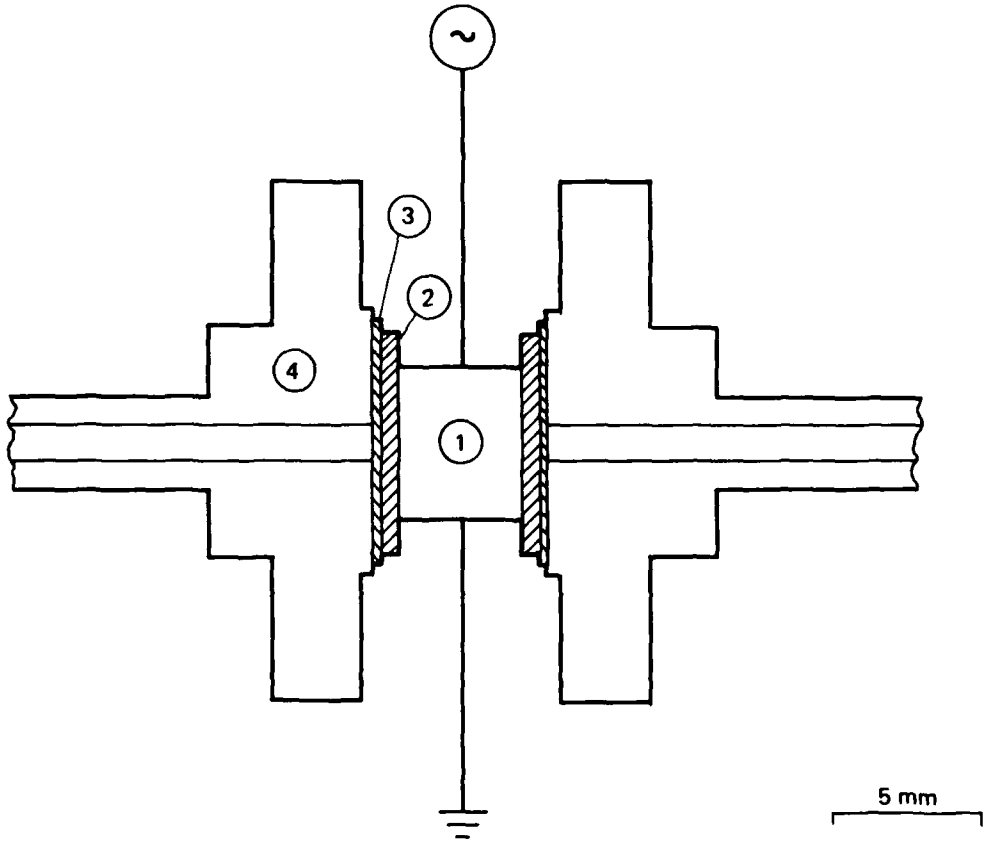

Figure 9. Sample mounting for phase shift measurement. 1 = sample crystal, 2 = quarter-wave plates, 3 = Kapton insulation, 4 = waveguide flange.

linear material, e.g., $BaTiO_3$) or at double the applied frequency (for the case of a quadratic material; e.g., KTN). The fractional modulation can then be related directly to the peak phase shift, which in turn is related to the effective electro-optic coefficient through Equation (2).

Our measurements in $BaTiO_3$ (at a modulation frequency of 200 Hz) yielded a linear electro-optic coefficient,

$$r_{33} = 3.8 \times 10^{-8} \text{ cm/V},$$

or

$$n^3 r_{33} = 1.6 \times 10^{-5} \text{ cm/V}.$$

These values are approximately 10 times larger than those for $LiNbO_3$ and $LiTaO_3$ at a carrier frequency of 94 GHz,[7] and are among the largest reported in any material. The applicability and importance of $BaTiO_3$ for practical devices will be discussed in Section VI.

While no electro-optic measurements of $BaTiO_3$ at millimeter wavelengths have been performed previously, the nonlinear coefficient d_{33} has been measured.[1] Using the relation $r=4d/(\chi_i)^2$, where χ_i is the ionic susceptibility,[1,13] we find

$$r_{33} = 1.4 \times 10^{-8} \text{ cm/V},$$

which is in good agreement with the value we have measured, considering the difference in the two experiments. We note also that our sample may have some residual 180^0 domains, which could lead to an underestimation of the electro-optic coefficient in a modulation experiment.[14] We estimate that this uncertainty is no more than 10%.[14]

Our measurements in KTN at the same modulation and carrier frequency yielded a quadratic electro-optic coefficient,

$$g_{11} = 0.06 \text{ m}^4/\text{C}^2.$$

While no previous measurements of g_{11} for KTN have been reported at millimeter wavelengths, we may compare our measured value with values measured at carrier frequencies in the visible spectral region.[15] This comparison is valid because the g-coefficient is known to be insensitive to temperature and frequency over a very wide range, and is even invariant from material to material among the perovskites.[15] For KTN in the visible the measured value is $g_{11}=0.14\ m^4/C^2$, in reasonable agreement with our measured value at 94 GHz.

SECTION VI

APPLICATION TO PRACTICAL DEVICES

Based on our measurements of the linear and electro-optic properties of $BaTiO_3$ at millimeter wavelengths, we wish to analyze the usefulness of this material for practical devices. We have considered this problem in several recent publications[12,13] and our ONR proposals.[11,16,17] It is worth reconsidering this issue on the basis of our new data on $BaTiO_3$, and other recent data on BSKNN.[18]

For a plane wave incident on a modulator crystal with a linear electro-optic effect (and a transverse modulating electric field), the induced phase shift (see Equation 2) is given by

$$\Gamma = \pi L/\lambda \; n^3 r \; E,$$

where L is the active length, $n^3 r$ is the effective electro-optic coefficient, and E is the applied electric field. In an absorbing material, the appropriate figure of merit is the phase shift per absorption length. With $L=\alpha^{-1}$ (where α is the absorption coefficient), we obtain

$$\Gamma_\alpha = \pi/\lambda \; (n^3 r/\alpha) \; E,$$

where the material-related quantities are given in parenthesis. Obviously, a large value of the figure of merit, Γ_α, is favorable, with values of $\pi/2$ or more being acceptable for most devices.

For materials with known electro-optic and linear dielectric properties at high frequencies, the above relation can be used to calculate Γ_α. In Table 5, we have listed Γ_α for several promising electro-optic materials. An earlier form of this Table (before recent measurements on $BaTiO_3$ and BSKNN) appeared in our ONR

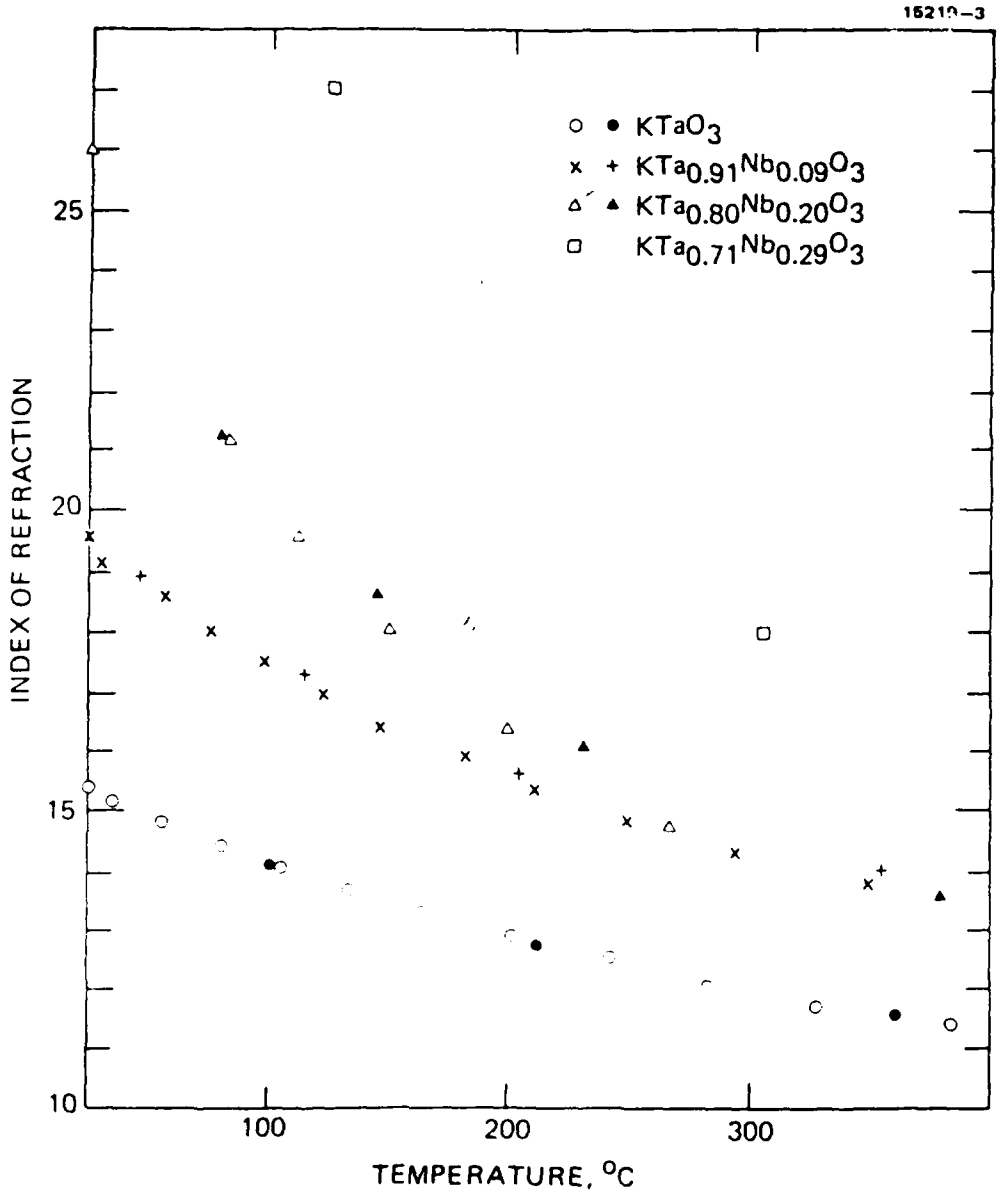

Fig. 3 :
Index of refraction at 94 GHz as a function of temperature for various $KTa_{1-x}Nb_xO_3$ crystals.

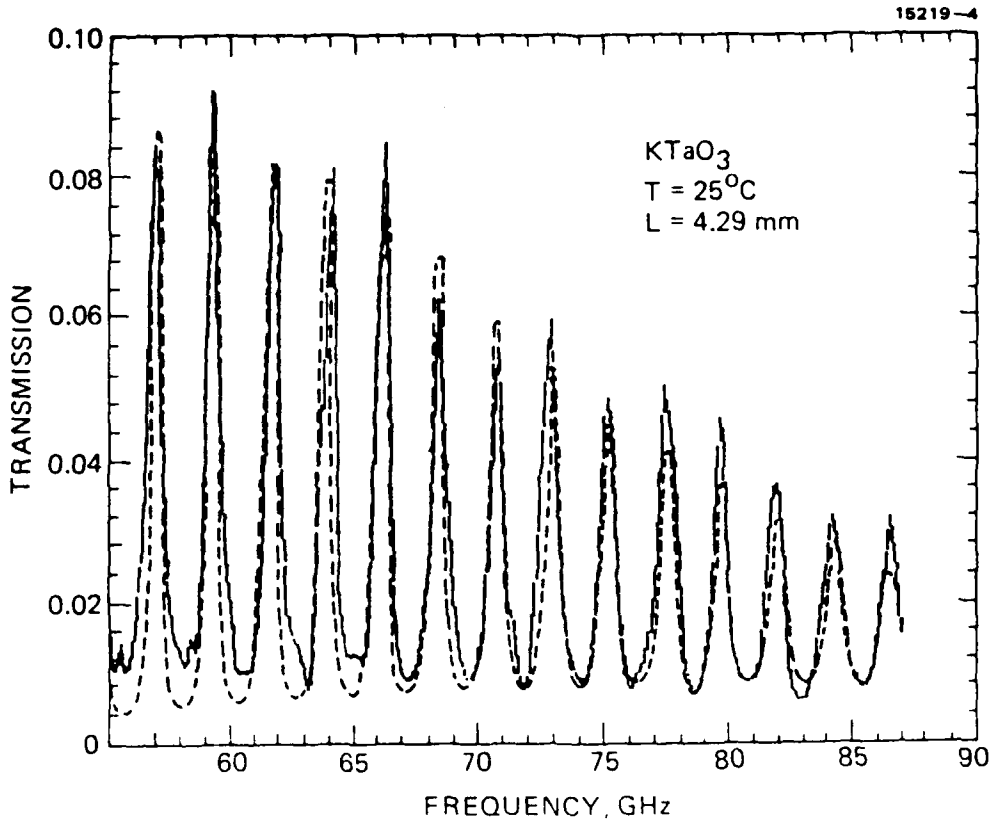

(a)

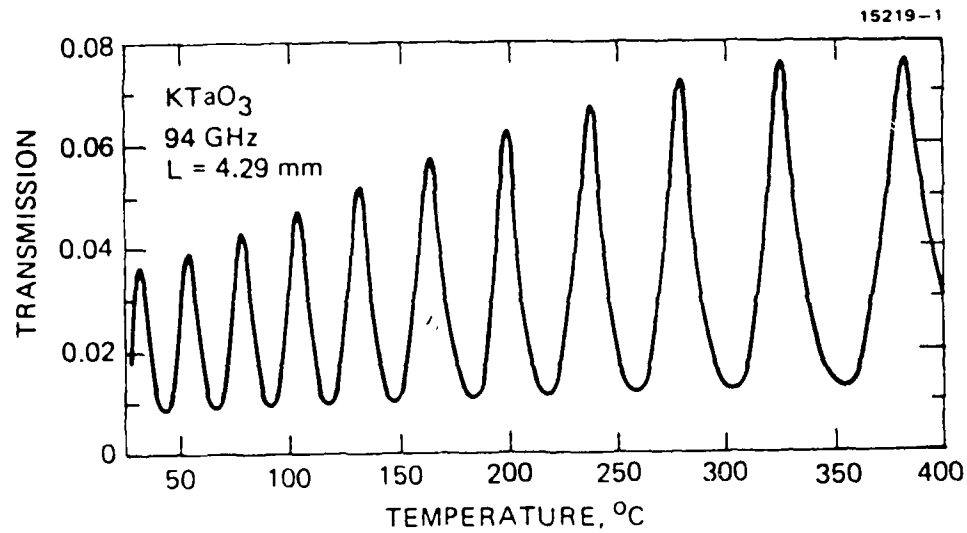

(b)

Fig. 2 :
Fabry-Perot spectra recorded with a $KTaO_3$ crystal having a thickness L = 4.29 mm :
(a) at room temperature as function of frequency. The solid segments connect experimental data points recorded every 0.2 GHz. The dotted curve is a theoretical fit obtained by using eq. (1).
(b) at 94 GHz as a function of temperature.

The phase factor $2\pi nL/\lambda$ has been varied in two different ways. In one experimental setup, using a backward wave oscillator as a variable frequency source, the wavelength λ was varied at room temperature. In the other setup, using a klystron as a fixed frequency source, we varied the temperature and thus the index of refraction n. The dielectric properties could be obtained at room temperature as a function of frequency in the range between 60 and 85 GHz or at a fixed frequency of 94 GHz for temperatures in the range 25 to 450°C.

3. RESULTS AND DISCUSSION

Typical measured fringe patterns are shown in Figure 2. Fabry-Perot spectra with excellent fringe visibility are obtained for measurements of the transmitted intensity both as a function of frequency and temperature. For every crystal, first the room temperature index of refraction n is determined from the peak spacing in the variable frequency measurement. Then the relative variation of n with temperature is obtained from the peak spacing in the fixed frequency measurement. Finally, the absorption coefficient α is determined from the peak transmission or from the contrast. Both values agree very well and give thus firm support to such a Fabry-Perot analysis. Finally, the loss tangent is obtained knowing n and α :

$$\tan \delta = \lambda\alpha/(2\pi n). \qquad (2)$$

The results obtained for KTN crystals with Nb concentrations between 0.29 and 0 are summarized in Figures 3 and 4 where the temperature dependences of the index of refraction and of the loss tangent at 94 GHz are given. In the temperature range investigated, it should be noted that the index of refraction obtained from static (at 1 kHz) dielectric measurements and the index measured at 94 GHz can be superimposed without any noticeable dispersion effects. Such effects should become

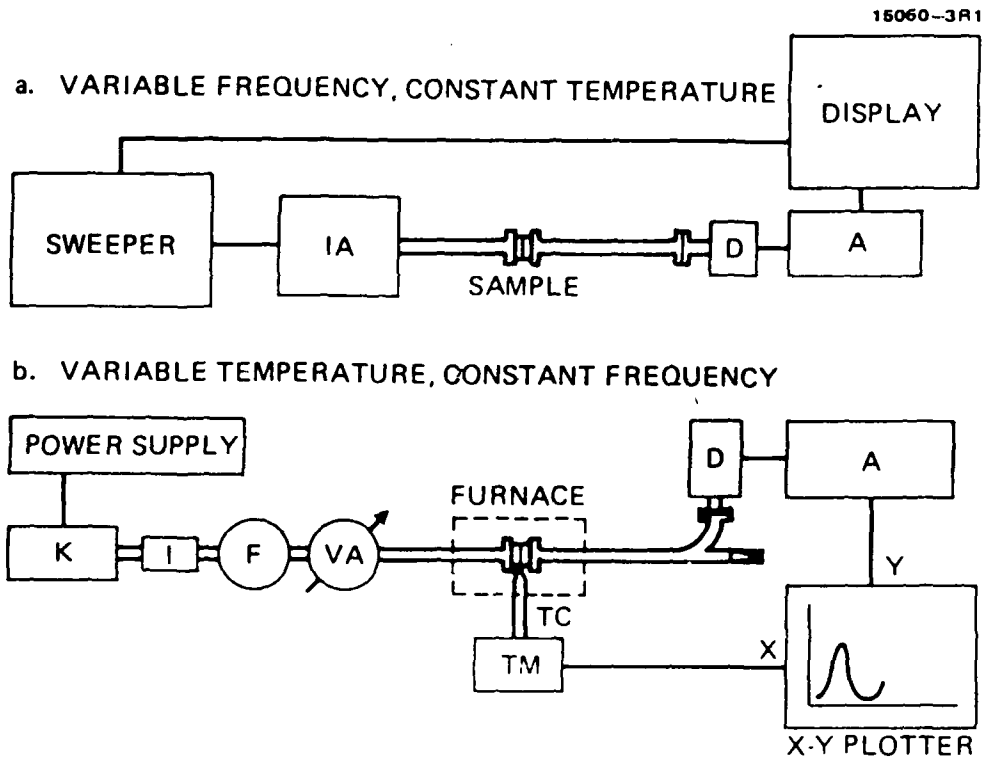

Fig. 1 :
Experimental setups for dielectric measurements at millimeter wavelengths, (a) at room temperature as a function of frequency; (b) at constant frequency as a function of temperature.
Symbols stand for : (D) detector, (IA) isolator and attenuator, (A) amplifier, (K) klystron, (I) isolator, (F) frequency-meter, (VA) variable attenuator, (TC) thermocouple, (TM) thermometer.

The experimental setup is schematically shown in Figure 1. The measurement technique utilizes samples with plane parallel faces mounted between the flanges of two standard rectangular metal waveguides. While measuring the transmission, the sample thus acts as a Fabry-Perot etalon, yielding a fringe pattern when the phase factor $2\pi nL/\lambda$ is varied (n is the millimeter wave refractive index and L is the sample thickness). The Fabry-Perot fringe pattern (in transmission, see Figure 2) is described by:

$$I_{transmitted}/I_{incident} = (1-R)^2\tau/[(1-R\tau)^2+4R\tau\sin^2(2\pi nL/\lambda)] \quad (1)$$

where R is the reflection coefficient, $\tau = \exp(-\alpha L)$, and α is the absorption coefficient. The coefficient R is taken as the Fresnel reflectivity from an air-to-dielectric interface, modified by the change in phase velocity resulting from the presence of the metallic waveguide walls [5]. For the samples decscribed here, high values of R in the range 0.8 to 0.9 are observed.

The use of free-standing samples eliminates the mechanical problems associated with mounting crystals inside the waveguide and facilitates the interchange of samples. By placing the samples in intimate contact with the waveguide flanges, diffraction effects are minimized. With this technique, high values of the dielectric constant ϵ ($\epsilon \simeq n^{1/2}$) and of the loss tangent can be accurately measured by using samples with sufficiently small thickness. Closely related techniques have been described in Ref. 6.

In order to obtain high quality Fabry-Perot patterns, two conditions have to be fulfilled. First, the free spectral range (i.e., the fringe spacing) has to be small enough so that at least two fringes are observed. Secondly, diffraction effects have to be small enough for the fringe shape to be well-defined. The latter condition is fulfilled when the Fresnel number characterizing the Fabry-Perot etalon $F = L\lambda/(nD^2)$, where D is determined by the aperture of the waveguide, is smaller than the empirically determined value $F_o \simeq 0.15$.

1. INTRODUCTION

Mixed crystals of $KTa_{1-x}Nb_xO_3$ or KTN are well known ferroelectrics whose transition temperatures T_c can be adjusted between -273 and 430°C by varying the Nb concentration x. In the past, KTN has attracted considerable interest due to its potential for electrooptic applications : adjusting T_c around 10 °C leads at room temperature to giant nonlinearities via the quadratic electrooptic effect [1]. Work at visible wavelengths has been hampered by compositional variations (i.e., striations) typical of most KTN crystals. Due to the empirically established fact that quadratic electrooptic coefficients are only very weakly dependent on frequency, temperature and material [2], one may expect the nonlinear effects to be important at millimeter wavelengths too. In this spectral range, striations which correspond to compositional fluctuations with periodicities on the scale 20 to 100 μm should not play a detrimental role.

It is therefore of interest to analyze the properties of KTN for different compositions at millimeter wavelengths. In the present work, we report on measurements of the dielectric constant and the loss tangent in the 60 to 95 GHz range as a function of temperature for concentrations x = 0.29, 0.20, 0.09, 0.025 and 0. Preliminary results of phase shifting experiments at 94 GHz are also presented.

2. EXPERIMENTAL

The growth of KTN crystals and the description of their phase transitions have been reported previously [3,4]. For the Nb concentrations indicated above, the paraelectric-to-ferroelectric phase transition takes place at -45, -103, -183 and -238°C, respectively (for x = 0, i.e. pure $KTaO_3$, there is no transition). The reason why no crystals with higher Nb concentrations and thus higher T_c's were investigated will become clear later.

APPENDIX A

DIELECTRIC PROPERTIES OF $KTa_{1-x}Nb_xO_3$ AT MILLIMETER WAVELENGTHS

D. Rytz, M.B. Klein, B. Bobbs*, M. Matloubian* and H. Fetterman*

Hughes Research Laboratories,
Malibu, California 90265, USA

*Dept. of Electrical Engineering, UCLA,
Los Angeles, California 90024, USA

Abstract - The dielectric constant and loss tangent of $KTa_{1-x}Nb_xO_3$ mixed crystals with $0<x<0.20$ are reported as a function of temperature and frequency at millimeter wavelengths.

Submitted for Conference Proceedings, Sixth International Meeting on Ferroelectricity, Kobe, Japan, August, 1985

18. B. Bobbs, H. Fetterman, M. Matloubian, R. Neurgaonkar, and W. Cory, "Electro-optic modulation of millimeter waves with cooled ferroelectrics," S.P.I.E. Technical Symposium East, April 9, 1985.

19. W. Ho, W.F. Hall, R.R. Neurgaonkar, R.E. DeWames, and T.C. Lim, Ferroelectrics 38, 833 (1981).

20. M.B. Klein, Int. J. Infrared and Millimeter Waves, 3, 587 (1982).

21. R. Clemens, G. Luther, and H.E. Muser, Phys. Stat. Sol. (a) 64, 637 (1981).

22. G. Burns, Phys. Lett. A43, 271 (1973).

23. G. Shirane, J.D. Axe, and J. Harada, Phys. Rev. B2, 3651 (1970).

24. M. Sparks, D.F. King, and D.L. Mills, Phys. Rev. B26, 6987 (1982).

25. A.S. Chaves, R.S. Katiyar, and S.P.S. Porto, Phys. Rev. B10, 3522 (1974).

26. J.A. Sanjuro, R.S. Katiyar, and S.P.S. Porto, Phys. Rev B22, 2396 (1980)

27. V. Belruss, J. Kalnajs, A. Linz, and R.C. Folweiler, Mat. Res. Bull. 6, 899 (1971).

28. Y. Luspin, J.L. Servoin, and F. Gervais, J. Phys. C 13, 3761 (1980).

REFERENCES

1. G.D. Boyd, T.J. Bridges, M.A. Pollack, and E.H. Turner, Phys. Rev Lett. 26, 387 (1971).

2. J.A. Basmajian and R.C. DeVries, J. Am. Ceram. Soc. 40, 373 (1957).

3. S. Ueda, Mat. Res. Bull. 9, 469 (1974).

4. K. Nassau and A.M. Broyer, J. Am. Ceram. Soc. 45, 474 (1962).

5. R.C. DeVries, J. Am. Ceram. Soc. 42, 547 (1959).

6. H. Arend and J. Novak, Kristall und Technik 1, 93 (1966).

7. M.B. Klein, Int. J. Infrared and Millimeter Waves 2, 239 (1981).

8. W.B. Bridges, M.B. Klein, and E. Schweig, IEEE Trans Microwave Theory and Techniques, MTT-30, 286 (1982).

9. I.Camlibel, M. DiDomenico, and S.H. Wemple, J. Phys. Chem. Solids 31, 1419 (1969).

10. S.H. Wemple, M. DiDomenico, and I. Camlibel, J. Phys. Chem. Solids 29, 1797 (1968).

11. M.B. Klein, "Nonlinear Materials For The Millimeter Spectral Region," ONR Proposal, October, 1981.

12. M.B. Klein, Ferroelectrics 50, [633]/307, (1983).

13. M.B. Klein, "Dielectric waveguide electro-optic Devices," in Infrared and Millimeter Waves, K. Button, Ed. (Academic Press, New York, 1983).

14. M.B. Klein and G.C. Valley, J. Appl. Phys. 57, 4901 (1985).

15. J.E. Geusic, S.K. Kurtz, L.G. Van Uitert, and S.H. Wemple, Appl. Phys. Lett. 4, 141 (1964).

16. M.B. Klein, "Nonlinear Materials For The Millimeter Spectral Region," ONR Proposal, October 1982.

17. M.B. Klein, "Nonlinear Materials For The Millimeter Spectral Region," ONR Proposal, October 1983.

The major challenge in understanding the dielectric losses in $BaTiO_3$ and BST is the development of an accurate model of multiphonon absorption. We propose to do this with the help of an outside consultant, probably Marshall Sparks, an acknowledged expert in this technical area. The models we develop will be tested by comparing the frequency and temperature dependence of ϵ_c with that predicted from a variety of physical mechanisms.

C. PRACTICAL PHASE SHIFTERS IN $BaTiO_3$, BST AND KTN

On the basis of our electro-optic measurements in $BaTiO_3$ and KTN, we believe that these materials, along with BST, are promising for practical devices. We propose to measure the electro-optic properties of BST as it becomes available, and then design and construct practical laboratory-scale phase shifters using each of the above materials. The performance will be characterized and compared with analytical results. We will also consider frequency doubling measurements if the right source is available.

ACKNOWLEDGMENTS

We thank K. Kirby for performing thermal analysis measurements. We also thank Prof. H. Fetterman (UCLA) for making his equipment available for our room temperature dielectric constant measurements. These measurements were performed in cooperation with B. Bobbs and M. Matloubian.

crystals comprising a smaller fraction of the melt volume. Both of these factors are expected to result in a dramatic reduction of inclusions, thus improving crystal quality and allowing complete poling of the samples. We will also continue our RAP studies (both during and after growth), with the goal of eliminating OH^-, thereby possibly reducing the losses. The reduction of water using RAP may also reduce the Pt concentration in the melt by reducing its solubility.

B. ANALYSIS OF THE DIELECTRIC PROPERTIES OF BST AND $BaTiO_3$

During this program we developed a practical, accurate technique for the measurement of the dielectric properties of ferroelectrics at millimeter wavelengths. Our data for $BaTiO_3$ is in good agreement with other measured values, but open questions remain in comparing the data to theory; we feel that a full understanding of the physical origins of both the dielectric constant and the loss tangent is very important for future applications.

Except for a small change due to domain clamping, the dielectric constant at millimeter frequencies in $BaTiO_3$ is the same as the low frequency value; i.e., little dispersion is observed. In the very high frequency limit (near the TO mode frequency), the dielectric constant can be calculated from the phonon frequencies (typically obtained from Raman data; see Table 4). For $BaTiO_3$, such calculations give lower values of dielectric constant, and show no peak at temperatures in the vicinity of the paraelectric-to-ferroelectric phase transition. The absence of such a peak is in contradiction with low-frequency measurements which show a sharp peak at the transition temperature. We propose to repeat our dielectric measurements at higher frequencies in the hopes of accessing the region of dispersion which must exist between ~100 GHz and ~1000 GHz. We also hope to extend our measurements downward in frequency to the region of dispersion due to domain clamping; the goal is to relate the measured dispersion to an independent measurement of domain structure and density.

SECTION VII

CONCLUSIONS AND RECOMMENDATIONS FOR FUTURE WORK

On the basis of its large phase shifting figure of merit, we believe that $BaTiO_3$ is a strong candidate for incorporation into practical devices. While most of our measurements have been performed on commercial solution-grown crystals, the BST crystals under development at Hughes Research Laboratories hold the promise of still larger nonlinearities, along with the tailoring of samples to device needs.

The three major technical efforts incorporated into our recently completed program are (1) crystal growth, (2) measurement and evaluation of dielectric properties, and (3) measurement of electro-optic properties and application to practical devices. As discussed earlier, major technical advances were made in each area. Yet in each case more work remains to be done. A brief outline of future work is presented below; more details will be included in our follow-on proposal.

A. CRYSTAL GROWTH AND PROCESSING

In spite of the difficulty in poling our BST samples, we believe that further development of BST will make this material a viable alternative to commercial solution-grown $BaTiO_3$. Through control of parameters during and after crystal growth, we will be able to make samples tailored to our needs, an option which is not available from the commercial supplier of $BaTiO_3$. Furthermore, the lower transition temperature of BST and its higher value of static dielectric constant (see Table 1) suggest that its nonlinear properties should be somewhat larger than those of pure $BaTiO_3$.

The major thrust of our continued crystal growth efforts will be the use of a larger, more stable crystal growth furnace. This will allow the use of larger crucibles (100-200 cm^3), compared to the present crucible size (30 cm^3). The larger crucibles will in turn allow diameter control, and will result in

proposal, dated October, 1983.[17] The modulating field, E, is assumed to be 20 kV/cm, and the frequency is 94 GHz. The values of absorption coefficient, α, are obtained from the loss tangent values through the use of Equation (1).

As indicated in Table 4, the room temperature data for $LiNbO_3$ and $LiTaO_3$ are from Ref. 7. The data for $BaTiO_3$ are from the measurements described in this report. The linear properties of BSKNN are taken from Ref. 18, while the nonlinear parameters are obtained by scaling from the $BaTiO_3$ data, using the relationship $r \sim n^2$, as derived in our earlier work.[7,11,13] The data for SBN is taken from Ref. 19. In scaling the SBN data to 94 GHz, we have neglected any dispersion in n or tan δ, as might be expected due to dielectric relaxation. We have also included estimated parameters for $LiTaO_3$ at 20 K.

We see from Table 4 that at room temperature $BaTiO_3$ outperforms all other materials. Although cooling of BSKNN to 20 K does reduce the losses, the reduction in refractive index does not lead to a significant improvement in the figure of merit, Γ_α. In fact, if our extrapolations for $LiTaO_3$ are accurate, we would expect this material to be much better than any of the others at 20 K.

A complete discussion of practical device configurations using electro-optical materials is given in References 13 and 20. In our opinion the most promising approach to the realization of practical devices is to incorporate the electro-optic material into the circuit in the form of a dielectric waveguide. We have designed and tested several waveguide devices based on $LiNbO_3$ (Ref. 13 and 20); their performance was very close to that calculated from the basic material properties.

For $BaTiO_3$ (with α=2-3 cm^{-1}), the optimum device length given by $L=\alpha^{-1}$, is 3 to 5 mm. This leads to the promise of very compact devices, as compared to $LiNbO_3$ and $LiTaO_3$, with $\alpha^{-1} \simeq$20-50 mm.

Table 5. Phase Shifting Figure of Merit Γ_α at 94 GHz for Several Promising Materials

15180-1R2

MATERIAL	ORIENTATION	REFRACTIVE INDEX n	DIELECTRIC CONSTANT ϵ	LOSS TANGENT TAN δ	ABSORPTION COEFFICIENT α (cm^{-1})	ELECTRO-OPTIC COEFFICIENT n^3r (cm/v)	FIGURE OF MERIT Γ_α (rad)	COMMENTS
$LiNbO_3$ (300 K)	333	5.2	27	0.002	0.2	5.0×10^{-7}	0.5	REF. 7
	113	6.7	45	0.004	0.2	4.8×10^{-7}	0.5	
	222	6.7	45	0.004	0.2	5.7×10^{-7}	0.6	
$LiTaO_3$ (300 K)	113	6.5	42	0.004	0.4	5.2×10^{-7}	0.3	
	333	6.5	42	0.007	0.9	1.5×10^{-6}	0.3	
(20 K)	333	~6.0	~36	$\sim 10^{-4}$	~0.01	$\sim 5.0 \times 10^{-7}$	~10	EXTRAPOLATED VALUES
BSKNN (300 K)	333	7.2	52	0.180	25	$\sim 1.3 \times 10^{-5}$	~0.1	REF. 18 (LINEAR PROPERTIES)
(20 K)	333	5.4	30	0.026	2.8	$\sim 3.1 \times 10^{-6}$	~0.2	n^3r EXTRAPOLATED FROM $BaTiO_3$
$BaTiO_3$ (300 K)	333	7.5	57	0.024	3.6	1.6×10^{-5}	0.9	ONR RESULTS
SBN (300 K)	–	~20 (a)	~400 (a)	~0.05 (a)	~15 (b)	1.2×10^{-4} (c)	~0.6	REF. 19

a. MEASURED AT 35 GHz

b. EXTRAPOLATED TO 94 GHz

c. MEASURED AT 58 GHz

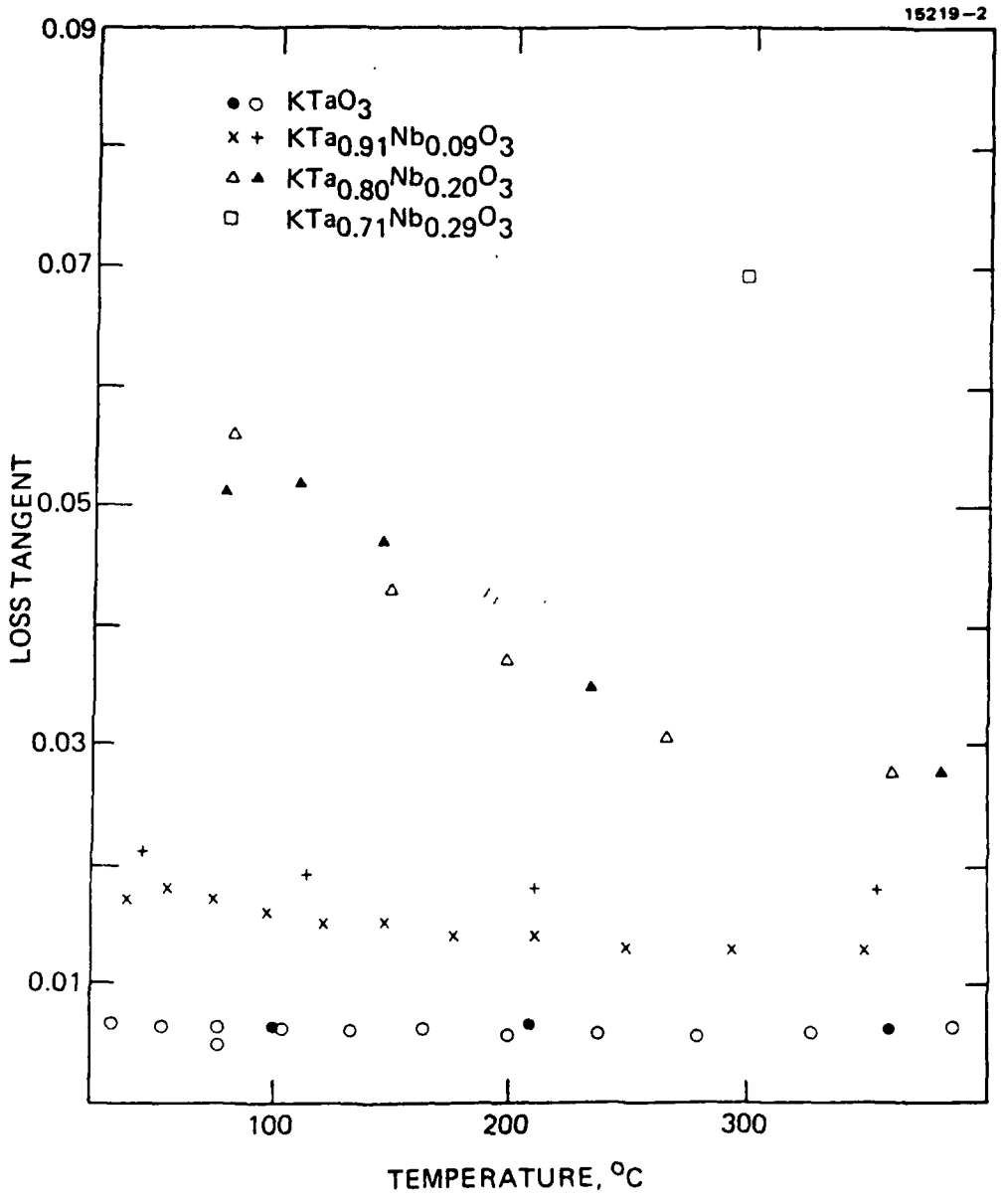

Fig. 4 :
Loss tangent at 94 GHz as a function of temperature for various $KTa_{1-x}Nb_xO_3$ crystals.

increasingly important on approaching T_c. However, due to the rapidly increasing losses when lowering the temperature closer to T_c, the fringe contrast becomes very poor. Therefore, the measurements have been restricted to limited concentration and temperature ranges. For the presently investigated KTN crystals, values of n between 15 and 26 and tan δ between 0.006 and 0.06 were obtained.

The electrooptic phase shift at 94 GHz has been measured in cubic KTN with x = 0.09 using the bridge technique described in Ref. 7. In order to avoid large reflections at the crystal surface, quarter-wave matching plates were mounted between the crystal and the metal waveguide. The crystal had electrodes such that an electric field could be applied with its direction parallel to the polarization of the incident millimeter radiation. The phase shift Γ is then given by :

$$\Gamma = n^3 \, g_{11} \, (\epsilon_o \epsilon E)^2 \, \pi L/\lambda \qquad (3)$$

where g_{11} is a quadratic electrooptic coefficient, ϵ_o the vacuum dielectric permittivity and E the electric field. Using the value n = 19.1 as previously measured and $g_{11} = 0.14 \ m^4/C^2$ as determined for visible wavelengths [1], a phase shift $\Gamma = 10^{-3}$ is predicted. A somewhat smaller (by a factor of 2 or 3) shift has been observed in the present experiments. New experiments aimed at measuring the quadratic electrooptic coefficients with improved accuracy at millimeter wavelengths are in progress.

4. SUMMARY

Optical constants can be measured at millimeter wavelengths by a Fabry-Perot transmission technique. This technique has been utilized for KTN crystals in the present work. Our measurements

have been performed for Nb concentrations in the range between 0 and 0.29 (for ferroelectric transition temperatures between -238 and -45°C) and cover temperature and frequency ranges between 25 and 450°C and between 60 and 94 GHz, respectively. The Fabry-Perot technique yields accurate results for refractive indices and loss-tangents as high as n = 26 and tan δ = 0.06. Preliminary results on quadratic electrooptic coefficients at 94 GHz have also been given.

ACKNOWLEDGMENT

One of the authors (DR) acknowledges financial support from the Swiss National Science Foundation.

REFERENCES

1. F.S. Chen, J.E. Geusic, S.K. Kurtz, J.G. Skinner and S.H. Wemple, J. Appl. Phys. 37, 388 (1966).

2. S.H. Wemple and M. DiDomenico, Electrooptical and Nonlinear Optical Properties of Crystals, in Applied Solid State Science (ed. by R. Wolfe) 3, 263 (1972).

3. D. Rytz and H.J. Scheel, J. Crystal Growth 59, 468 (1982).

4. D. Rytz, PhD Thesis, Swiss Federal Institute of Technology, Lausanne, Switzerland, unpublished (1983).

5. W.B. Bridges, M.B. Klein and E. Schweig, IEEE Trans. MTT-30, 468 (1982).

6. G.V. Kozlov, A.M. Prokhorov and A.A. Volkov, Submillimeter Dielectric Spectroscopy of Solids, in Problems in Solid-state Physics (ed. by A.M. Prokhorov and A.S. Prokhorov), Mir, Moscow (198), p. 14.

7. M.B. Klein, Int. J. Infrared and Millimeter Waves 2, 239 (1981).

APPENDIX B

DIELECTRIC PROPERTIES OF CUBIC $Ba_{1-x}Sr_xTiO_3$ (x=0.025) AT 94 GHz

D. Rytz, B.A. Wechsler and M.B. Klein
Hughes Research Laboratories
Malibu, Ca 90265

Mixed $Ba_{1-x}Sr_xTiO_3$ ("BST") becomes cubic above T_c = 119°C for a strontium concentration, x = 0.025. These figures should be compared to T_c = 131-134°C for top-seeded-solution-grown crystals (Johnson 1965) and T_c = 120°C for KF-flux grown crystals (Merz 1949). Dielectric measurements on cubic $BaTiO_3$ can be found in the literature for crystals grown by both techniques over a frequency range of 1 kHz to 75 GHz. Table 1 gives an overview of these results.

In the present work, measurements of the dielectric constant and loss tangent of BST with x = 0.025 are reported for the temperature range 200 to 550°C at 94 GHz. These crystals were grown by a modified Czochralski technique and T_c was determined by differential scanning calorimetry. The dielectric measurement technique utilizes samples with plane parallel faces mounted between the flanges of two standard rectangular waveguides. The sample thus acts as a Fabry-Perot etalon and fringes are obtained when the phase factor $2\pi nL/\lambda$ is varied (n is the microwave refractive index, λ is the wavelength of the incident wave, and L is the thickness of the sample). A typical fringe pattern is shown in Figure 1 for two samples of different thickness, L = 0.14 and 0.50 mm, respectively. The relative variation of n is obtained from the fringe spacing. In order to determine the absolute value of n at a given temperature, we used the dielectric constant measured by Rupprecht and Bell (1964) as a calibration because their Curie-Weiss law reproduces our experimentally determined variation of n fairly well. Our results, together with data from the literature, are summarized in Figure 2. In the temperature range of interest, the shift in T_c due to the addition of strontium is apparently irrelevant for

Table 1. Dielectric Constant and Loss Tangent of cubic $BaTiO_3$

15253–7

REFERENCE	CURIE-WEISS LAW (T IN °C)	T = 160	T = 220
JOHNSON 1965 (1 kHz)	ϵ = 150000/(T-115)	3330	1430
CAMLIBEL ET AL. 1969 (1 kHz AND 75 MHz)	ϵ = 180000/(T-112)	3750	1670
BENEDICT AND DURAND 1958 (24 GHz)		2300	
RUPPRECHT AND BELL 1964 (8.2-12.4 GHz)	ϵ = 44+120000/(T-123)	3290	1280
POLPAVKO ET AL. 1968 (75 GHz)		1800	1100
KAATZE 1972 (25 GHz)		2200	

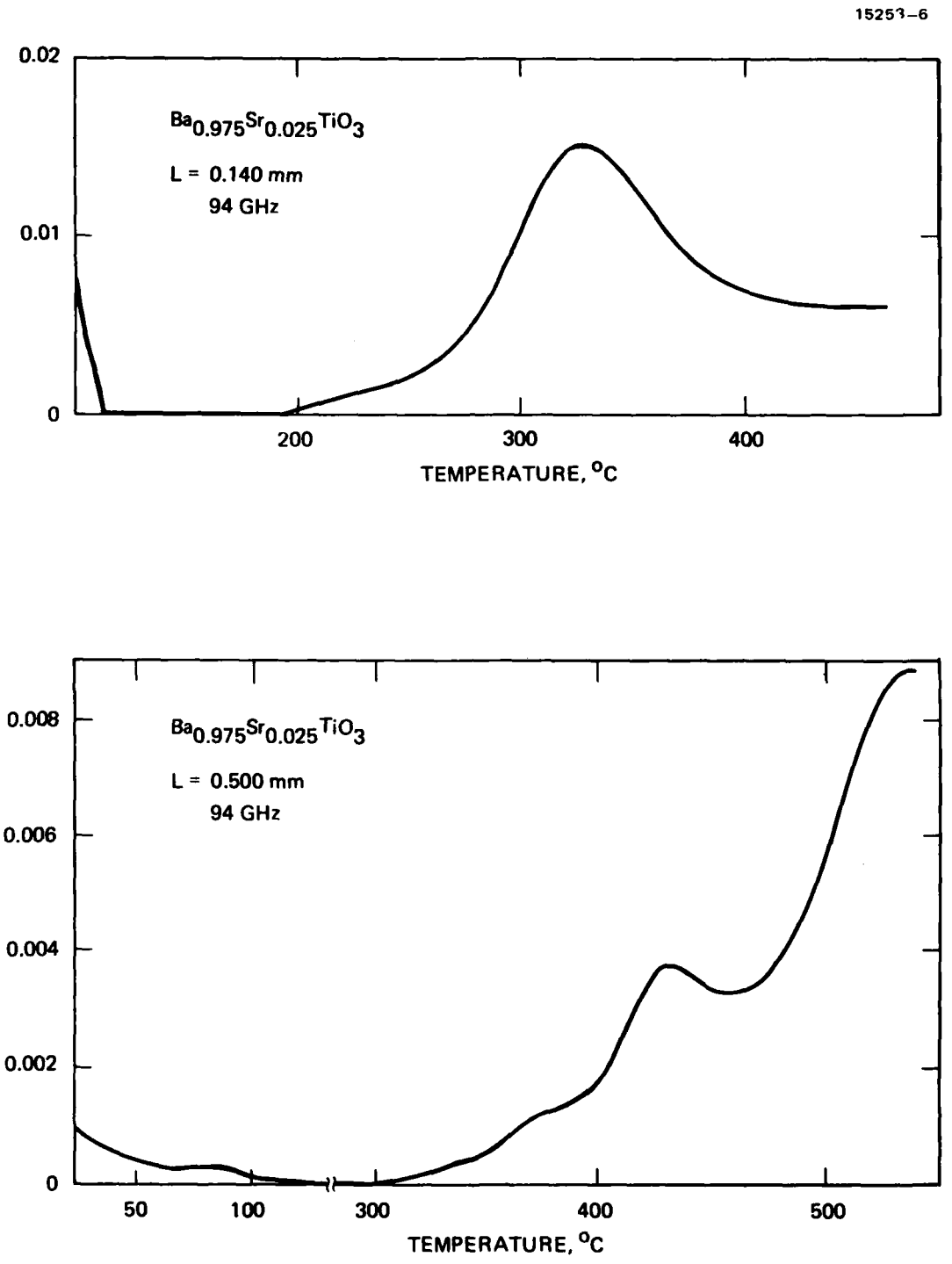

Figure 1. Temperature dependence of the transmission at 94 GHz in $Ba_{0.975}Sr_{0.025}TiO_3$.

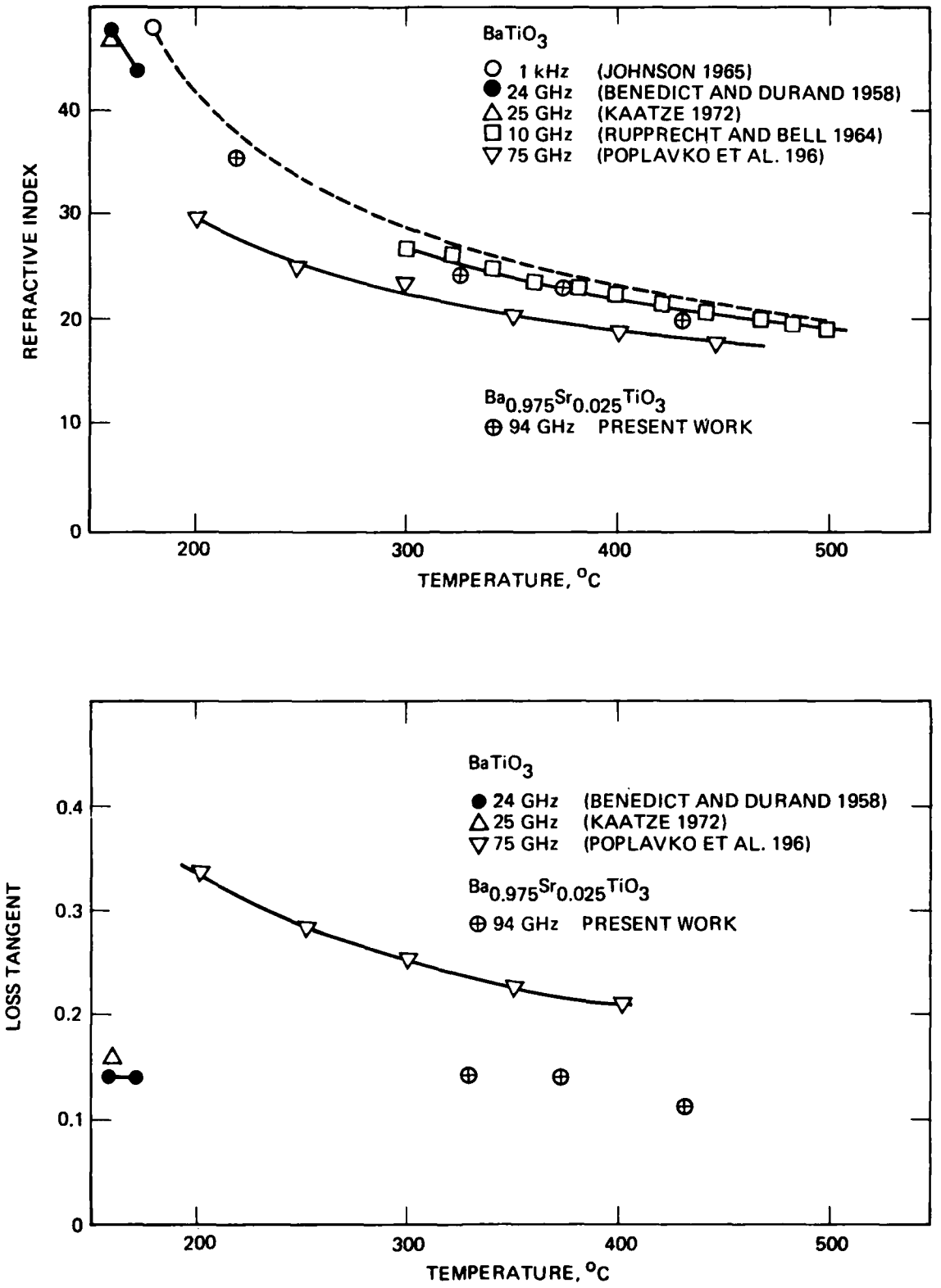

Figure 2. Temperature dependence of the refractive index and the loss tangent.

the different crystals, as can be deduced from the qualitative agreement for the 1 kHz to 10 GHz and 94 GHz curves. The index of refraction obtained at 75 GHz by Poplavko et al. (1968) is much too low and was probably measured with samples of unknown impurity content.

From our refractive index measurements, we conclude that there is a detectable dispersion at even 100 to 450°C above T_c. This dispersion seems much smaller however than what might be inferred from the data by Poplavko et al. (1968).

Due to the high absorption of BST in the investigated temperature range, very thin samples have to be used and the fringe contrast is poor. Nevertheless, the loss tangent could be obtained from

$$\tan \delta = \lambda\alpha/(2\pi n) \quad , \tag{1}$$

where α, the absorption coefficient, is determined from the contrast or the peak transmission. The resulting values of tan δ are displayed in Figure 2. They are in the range 0.11 to 0.14 and are thus close to the values obtained by Benedict and Durand (1958) and Kaatze (1972) at 24 GHz. The loss tangent measured at 75 GHZ by Poplavko et al. (1968) is nearly a factor of two higher, a discrepancy which again points at a major difference in sample quality.

These measurements demonstrate the usefulness of the Fabry-Perot resonator technique for dielectric measurements, even in highly absorbing materials such as cubic $Ba_{1-x}Sr_xTiO_3$.

REFERENCES

I. Camlibel, M. DiDomenico and S.H. Wemple, J. Phys. Chem. Solids 31 1419 (1969).

C.J. Johnson, Appl. Phys. Lett. 7 221 (1985).

U. Kaatze, Phys. Stat. Sol. b50 537 (1972).

W. Merz, Phys. Rev. 76 1221 (1949).

E. Nakamura and J. Furuichi, J. Phys. Soc. Japan 15 1955 (1960).

Yu. M. Poplavko, V.G. Tsykalov, and V.I. Molchanov, Fiz. Tverd. Tela 10 3425 (1968) (Sov. Phys.-Solid State 10 2708 (1968)).

G. Rupprecht and R.O. Bell, Phys. Rev. 135 A748 (1964).

END

FILMED

11-85

DTIC